ISSN 0287-9808
KURRI-TR-447
ONLINE ISSN 2189-7115
ONLINE ETR- 1

京都大学臨界集合体実験装置における 100 MeV 陽子を用いた加速器駆動システムの固体 Pb-Bi の中性子特性に関する実験ベンチマーク

Experimental Benchmarks of Neutronics on Solid Pb-Bi in Accelerator-Driven System with 100 MeV Protons at Kyoto University Critical Assembly

編集：卞　哲浩
Edited by **:** Cheol Ho Pyeon

京 都 大 学 原 子 炉 実 験 所
Research Reactor Institute, Kyoto University

Preface

These experimental benchmarks were contributed to the Coordinated Research Project (CRP) T33002 in the International Atomic Energy Agency (IAEA), as entitled "**Accelerator Driven Systems (ADS) and Use of Low-Enriched Uranium in ADS**," from 2016 to 2018.

The main objective of these benchmarks is to contribute to research and development of Pb-Bi neutronics in ADS through the experimental data with the use of spallation neutrons generated by 100 MeV protons and Pb-Bi target carried out at the Kyoto University Critical Assembly (KUCA) A-core.

Special thanks are due the KUCA and the fixed-filed alternative gradient (FFAG) accelerator staff and students for support and patience throughout a series of ADS experiments carried out at KUCA.

Cheol Ho Pyeon

June 2017

Keywords:
ADS, KUCA, FFAG accelerator, Spallation neutrons, Pb-Bi

要　旨

この実験ベンチマーク問題は、国際原子力機関（IAEA）において 2016 年から 2018 年にかけて行われた国際共同研究プロジェクト T33002「加速器駆動システム（ADS）と ADS における低濃縮ウラニウムの利用」の一部として採択された「京都大学臨界集合体実験装置における 100 MeV 陽子を用いた加速器駆動システムの固体 Pb-Bi の中性子特性に関する実験ベンチマーク」である。

この実験ベンチマーク問題は、KUCA の A 架台において行われた FFAG 加速器から得られる核破砕中性子を用いた実験を通して、ADS における Pb-Bi の基礎研究の発展に貢献することを目的としている。

最後に、KUCA において ADS 実験を準備および運転にご協力をいただいた KUCA および FFAG 加速器のスタッフ、実験における測定および数値解析に献身的に取り組んだ KUCA 棟に在籍していた学生諸君に心から感謝の意を表します。

卞　哲浩

2017 年 6 月

Contents

Experimental Benchmarks of Neutronics on Solid Pb-Bi in Accelerator-Driven System with 100 MeV Protons at Kyoto University Critical Assembly

目　次

京都大学臨界集合体実験装置における 100 MeV 陽子を用いた加速器駆動システムの固体 Pb-Bi の中性子特性に関する実験ベンチマーク

Experimental Benchmarks of Neutronics on Solid Pb-Bi in Accelerator-Driven System with 100 MeV Protons at Kyoto University Critical Assembly

Research Reactor Institute, Kyoto University, Japan

Cheolho Pyeon

Phase I

Study on Target (W, W-Be and Pb-Bi)

1. Collaborative Work Specifications

1-1. Introduction

The accelerator-driven system (ADS) was developed for producing energy and for transmuting minor actinides and long-lived fission products. ADS has attracted worldwide attention in recent years because of its superior safety characteristics and potential for burning plutonium and nuclear waste. An outstanding advantage of its use is the anticipated absence of reactivity accidents, provided sufficient subcriticality is ensured. At the Kyoto University Research Reactor Institute (KURRI) [1]-[2], a series of experiments on ADS was launched in fiscal 2003 at the Kyoto University Critical Assembly (KUCA) [3]-[26], with sights on a future plan (**K**umatori **A**ccelerator Driven **R**eactor **T**est Facility **&** Innovation Research **Labo**ratory: Kart & Lab. Project). A new accelerator was attached to the KUCA facility in March 2008, and the high-energy neutrons generated by the interaction of 100 MeV protons with tungsten target was injected into KUCA. The new accelerator is called the fixed-field alternating gradient (FFAG) [27]-[28] accelerator of the synchrotron type developed by High Energy Accelerator Research Organization (KEK) in Japan.

The experimental studies on ADS are being conducted for nuclear transmutation analyses with the combined use of KUCA and the FFAG accelerator, KURRI. The ADS experiments [17]-[26] with 100 MeV protons obtained from the FFAG accelerator had been carried out to investigate the neutron characteristics of ADS, and the static and kinetic parameters were accurately analyzed through both the measurements and the Monte Carlo simulations of reactor physics parameters, including the reaction rates, the neutron spectrum, the neutron multiplication, the neutron decay constants and the subcriticality. In addition to the uranium-loaded core, the spallation neutrons generated by 100 MeV proton beams from the FFAG accelerator had been also injected into the thorium-loaded core [21]-[22] to conduct the feasibility studies on the thorium-loaded ADS through the experimental analyses of the static conditions and kinetic behaviors.

In this study, attention was paid to the influences of different source neutron spectrum on the core characteristics [25]: the neutron multiplication and the subcritical multiplication factor were obtained differently with the use of solid two-layer (W-Be) and solid Pb-Bi targets, compared with the W target (reference target at KUCA). Note that the Pb-Bi target was consisted of a mixture ratio of 44.5% (Pb) and 55.5% (Bi). Then the high-energy neutrons caused by the neutron yield at the location of target were attained in the injection of 100 MeV protons into these targets. Also kinetic parameters of prompt neutron decay constant and subcriticality were experimentally estimated, when the source neutron spectrum was varied by the kind of solid target. The objective of this study was to investigate experimentally the neutron characteristics of solid targets in the ADS experiments with 100 MeV protons, when the neutron spectrum in high-energy region and the neutron yield of high-energy neutrons were acquired with the use of the solid targets, through the static and kinetic experiments, and to evaluate the accuracy of the Monte Carlo analyses through the calculations by the MCNP6 [29] code with JENDL-4.0 [30] for transport, JENDL/HE-2007 [31]-[32] for high-energy protons and neutrons, and JENDL/D-99 [33] libraries for reaction rates.

1-2. Experimental Settings

1-2-1. Description of KUCA core

KUCA comprises solid-moderated and -reflected type-A and -B cores, and a water-moderated and -reflected type-C core. In the present series of experiments, the solid-moderated and -reflected type-A core was combined with a Cockcroft-Walton type pulsed neutron generator and the FFAG accelerator at KUCA.

The A-core (A1/8”P60EUEU(3)) configuration used for measuring the reaction rates is shown in Fig. 1-1. The fuel rods were constructed of a combination of 25 elements that were loaded on the grid plate. The materials used in the critical assemblies were always in the form of rectangular parallelepipe, 2” sq. with thickness ranging between 1/16” and 2”. The upper and lower parts of the fuel region were polyethylene reflector layers of more than 500 mm long, as shown in Fig. 1-2. The fuel rod, a highly-enriched uranium-aluminum (U-Al) alloy, consisted of 60 cells of polyethylene plate 1/8” thick, and a U-Al plate 1/16” thick and 2” sq. The functional height of the core was approximately 400 mm.

1-2-2. Description of FFAG accelerator

100 MeV protons generated from the FFAG accelerator were injected onto the heavy metal target (W, W-Be and Pb-Bi). The main characteristics are under the following parameters: 100 MeV energy, 1 nA intensity, 20 Hz pulsed frequency, 100 ns pulsed width and 40 mm diameter spot size at the target. The thickness of target was determined on the basis of previous analyses [15], [19] in the reaction rates for high-energy protons. A level of the neutron yield generated at the target was around 1.0×10^{8} 1/s by an injection of 100 MeV protons onto the heavy metal target.

1-3. Experimental Results

1-3-1. Indium (In) reaction rate distribution

Indium (In) wire 1.0 mm diameter and 800 mm long was set in the axial center position along (17, 16 - P, A') the vertical direction shown in Fig. 1-1 for measuring the reaction rate distribution. The experimental results of the In wire were obtained by measuring total counts of the peak energy of γ-ray emittance and normalized by the counts of irradiated In foil (10*10*1 mm) emitted from ^{115}In(n, n')^{115m}In (threshold energy 0.3 MeV) reactions set at the location of the target.

1-3-2. Time evolution data of PNS and Noise methods

For 100 MeV protons, to monitor carefully the prompt and delayed neutron behaviors, each core was set with two BF_3 detectors (1/2" and 1" diameters; 300 mm long) at the axial central positions of #1 in (10, U) and #2 in (15, X), respectively, and an optical fiber in (16-15, O-P), as shown in Fig. 1-1. Through the time evolution data of prompt and delayed neutrons, the prompt neutron decay constant was deduced by the least-square fitting of the time evolution of the neutrons to an exponential function over the time optimal duration. Subcriticality was deduced by the extrapolated area ratio method on the basis of the prompt and delayed neutron behaviors.

1-3-3. Critical position and Excess reactivity

The critical state was adjusted by maintaining the control rods in certain positions, and the excess reactivity was attained on the basis of its integral calibration curve obtained by the positive period method.

Table 0 List of experimental data in all the cores

Case	Number of fuel rods	Rod insertion	100 MeV protons		
			Indium reaction rate distribution	PNS method	Noise method
Case I-1	25	C1, C2, C3	-	Available	Available
Case I-2	25	C1, C2, C3, S4	-	Available	Available
Case I-3	25	C1, C2, C3, S4, S5, S6	Available	Available	Available
Case I-4	21	All six rods withdrawn	-	Available	Available
Case I-5	21	C1, C2, S4, S6	-	Available	Available

1-4. References

[1] S. Shiroya, H. Unesaki, Y. Kawase, H. Moriyama and M. Inoue, "Accelerator Driven Subcritical System as a Future Neutron Source in Kyoto University Research Reactor Institute (KURRI) – Basic Study on Neutron Multiplication in the Accelerator Driven Subcritical Reactor," *Prog. Nucl. Energy*, **37**, 357 (2000).

[2] S. Shiroya, A. Yamamoto, K. Shin, T. Ikeda, S. Nakano and H. Unesaki, "Basic Study on Accelerator Driven Subcritical Reactor in Kyoto University Research Reactor Institute (KURRI)," *Prog. Nucl. Energy*, **40**, 489 (2002).

[3] C. H. Pyeon, Y. Hirano, T. Misawa, H. Unesaki, C. Ichihara, T. Iwasaki and S. Shiroya, "Preliminary Experiments on Accelerator Driven Subcritical Reactor with Pulsed Neutron Generator in Kyoto University Critical Assembly," *J. Nucl. Sci. Technol.,* **44**, 1368 (2007).

[4] C. H. Pyeon, M. Hervault, T. Misawa, H. Unesaki, T. Iwasaki and S. Shiroya, "Static and Kinetic Experiments on Accelerator Driven Subcritical Reactor with 14 MeV Neutrons in Kyoto University Critical Assembly," *J. Nucl. Sci. Technol.,* **45**, 1171 (2008).

[5] C. H. Pyeon, H. Shiga, T. Misawa, T. Iwasaki and S. Shiroya, "Reaction Rate Analyses for an Accelerator-Driven System with 14 MeV Neutrons in Kyoto University Critical Assembly," *J. Nucl. Sci. Technol.*, **46**, 965 (2009).

[6] H. Shahbunder, C. H. Pyeon, T. Misawa and S. Shiroya, "Experimental Analysis for Neutron Multiplication by using Reaction Rate Distribution in Accelerator-Driven System," *Ann. Nucl. Energy*, **37**, 592 (2010).

[7] H. Taninaka, K. Hashimoto, C. H. Pyeon, T. Sano, T. Misawa and T. Osawa, "Determination of Lambda-Mode Eigenvalue Separation of a Thermal Accelerator-Driven System from Pulsed Neutron Experiment," *J. Nucl. Sci. Technol.*, **47**, 376 (2010).

[8] H. Shahbunder, C. H. Pyeon, T. Misawa, J. Y. Lim and S. Shiroya, "Subcritical Multiplication Factor and Source Efficiency in Accelerator-Driven System," *Ann. Nucl. Energy*, **37**, 1214 (2010).

[9] H. Shahbunder, C. H. Pyeon, T. Misawa, J. Y. Lim and S. Shiroya, "Effects of Neutron Spectrum and External Neutron Source on Neutron Multiplication Parameters in Accelerator-Driven System," *Ann. Nucl. Energy*, **37**, 1785 (2010).

[10] H. Taninaka, K. Hashimoto, C. H. Pyeon, T. Sano, T. Misawa, H. Unesaki, W. Sugiyama and T. Osawa, "Determination of Subcritical Reactivity of a Thermal Accelerator-Driven System from Beam Trip and Restart Experiment," *J. Nucl. Sci. Technol.*, **48**, 873 (2011).

[11] H. Taninaka, A. Miyoshi, K. Hashimoto, C. H. Pyeon, T. Sano, T. Misawa, W. Sugiyama and T. Osawa, "Feynman-α Analysis for a Thermal Subcritical Reactor System Driven by an Unstable 14MeV-Neutron Source," *J. Nucl. Sci. Technol.*, **48**, 1272 (2011).

[12] C. H. Pyeon, Y. Takemoto, T. Yagi, Y. Takahashi and T. Misawa, "Accuracy of Reaction Rates in the Accelerator-Driven System with 14 MeV Neutrons at the Kyoto University Critical Assembly," *Ann. Nucl. Energy*, **40**, 229 (2012).

[13] A. Sakon, K. Hashimoto, W. Sugiyama, H. Taninaka, C. H. Pyeon, T. Sano, T. Misawa, H.

Unesaki and T. Ohsawa, "Power Spectral Analysis for a Thermal Subcritical Reactor System Driven by a Pulsed 14 MeV Neutron Source," *J. Nucl. Sci. Technol.*, **50**, 481 (2013).

[14] A. Sakon, K. Hashimoto, M. A. Maarof, M. Kawasaki, W. Sugiyama, C. H. Pyeon, T. Sano, T. Yagi and T. Ohsawa, "Measurement of Large Negative Reactivity of an Accelerator-Driven System in the Kyoto University Critical Assembly," *J. Nucl. Sci. Technol.,* **51**, 116 (2014).

[15] A. Sakon, K. Hashimoto, W. Sugiyama, S. Hohara, C. H. Pyeon, T. Sano, T. Yagi and T. Ohsawa, "Determination of Prompt-Neutron Decay Constant from Phase Shift between Beam Current and Neutron Detection Signals for an Accelerator-Driven System in the Kyoto University Critical Assembly," *J. Nucl. Sci. Technol.*, **52**, 204-213 (2015).

[16] T. Endo, A. Yamamoto, T. Yagi and C. H. Pyeon, "Statistical Error Estimation of the Feynman-α Method using the Bootstrap Method," *J. Nucl. Sci. Technol.*, **53**, 1447-1453 (2016).

[17] C. H. Pyeon, T. Misawa, J. Y. Lim *et al.*, "First Injection of Spallation Neutrons Generated by High-Energy Protons into the Kyoto University Critical Assembly," *J. Nucl. Sci. Technol.*, **46**, 1091 (2009).

[18] C. H. Pyeon, H. Shiga, K. Abe, H. Yashima, T. Nishio, T. Misawa, T. Iwasaki and S. Shiroya, "Reaction Rate Analysis of Nuclear Spallation Reactions Generated by 150, 190 and 235 MeV Protons," *J. Nucl. Sci. Technol.*, **47**, 1090 (2010).

[19] J. Y. Lim, C. H. Pyeon, T. Yagi and T. Misawa, "Subcritical Multiplication Parameters of the Accelerator-Driven System with 100 MeV Protons at the Kyoto University Critical Assembly," *Sci. Technol. Nucl. Install.*, **2012**, ID: 395878, 9 pages, (2012).

[20] Y. Takahashi, T. Azuma, T. Nishio, T. Yagi, C. H. Pyeon and T. Misawa, "Conceptual Design of Multi-Targets for Accelerator-Driven System Experiments with 100 MeV Protons," *Ann. Nucl. Energy*, **54**, 162 (2013).

[21] T. Yagi, C. H. Pyeon and T. Misawa, "Application of Wavelength Shifting Fiber to Subcriticality Measurements," *Appl. Radiat. Isot.*, **72**,11 (2013).

[22] C. H. Pyeon, T. Azuma, Y. Takemoto, T. Yagi and T. Misawa, "Experimental Analyses of External Neutron Source Generated by 100 MeV Protons at the Kyoto University Critical Assembly," *Nucl. Eng. Technol.*, **45**, 81 (2013).

[23] C. H. Pyeon, J. Y. Lim, Y. Takemoto, T. Yagi, T. Azuma, H. S. Kim, Y. Takahashi, T. Misawa and S. Shiroya, "Preliminary Study on the Thorium-Loaded Accelerator-Driven System with 100 MeV Protons at the Kyoto University Critical Assembly," *Ann. Nucl. Energy*, **38**, 2298 (2011).

[24] C. H. Pyeon, T. Yagi, K. Sukawa, Y. Yamaguchi and T. Misawa, "Mockup Experiments on the Thorium-Loaded Accelerator-Driven System in the Kyoto University Critical Assembly," *Nucl. Sci. Eng.*, **177**, 156-168 (2014).

[25] C. H. Pyeon, H. Nakano, M. Yamanaka, T. Yagi and T. Misawa, "Neutron Characteristics of Solid Targets in Accelerator-Driven System with 100 MeV Protons at Kyoto University Critical Assembly," *Nucl. Technol.*, **192**, 181-190 (2015).

[26] M. Yamanaka, C. H. Pyeon, T. Yagi and T. Misawa, "Accuracy of Reactor Physics Parameters in Thorium-Loaded Accelerator-Driven System Experiments at Kyoto University Critical Assembly," *Nucl. Sci. Eng.*, **183**, 96-106 (2016).

[27] J. B. Lagrange, T. Planche, E. Yamakawa *et al.*, "Straight Scaling FFAG Beam Line," *Nucl. Instrum. Methods A*, **691**, 55 (2013).

[28] E. Yamakawa, T. Uesugi, J. B. Lagrange *et al.*, "Serpentine Acceleration in Zero-Chromatic FFAG Accelerators," *Nucl. Instrum. Methods A*, **716**, 46 (2013).

[29] J. T. Goorley *et al.*, "Initial MCNP6 Release Overview – MCNP6 version 1.0," LA-UR-13-22934 (2013).

[30] K. Shibata, O. Iwamoto, T. Nakagawa *et al.*, "JENDL-4.0: A New Library for Nuclear Science and Engineering," *J. Nucl. Sci. Technol.*, **48**, 1 (2011).

[31] T. Fukahori, "JENDL High-Energy File," *J. Nucl. Sci. Technol.*, *suppl.*, **2**, 25 (2002).

[32] H. Takada, K. Kosako and T. Fukahori, "Validation of JENDL High-Energy File through Analyses of Spallation Experiments at Incident Proton Energies from 0.5 to 2.83 GeV," *J. Nucl. Sci. Technol.*, **46**, 589 (2009).

[33] K. Kobayashi, T. Iguchi, S. Iwasaki *et al.*, "JENDL Dosimetry File 99 (JENDL/D-99)," JAERI Report 1344, (2002).

Appendix-I

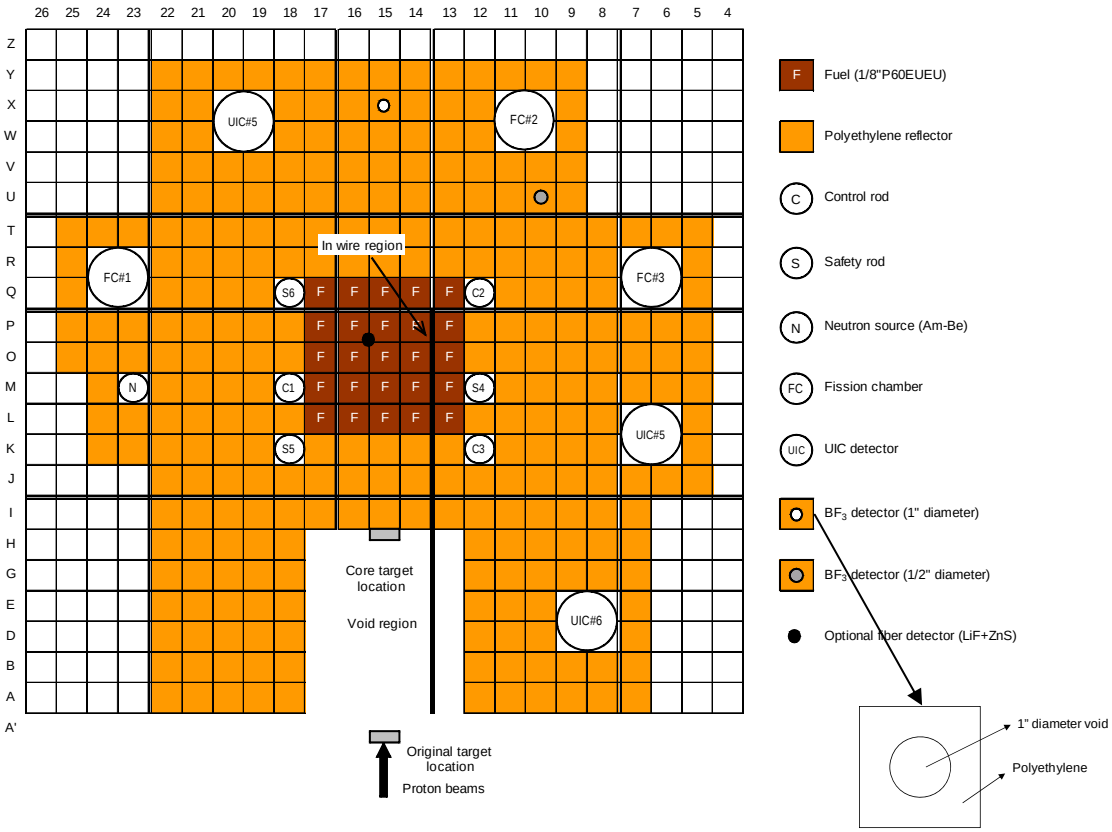

Fig. 1-1 The general view of KUCA core configuration (Ref. [25])

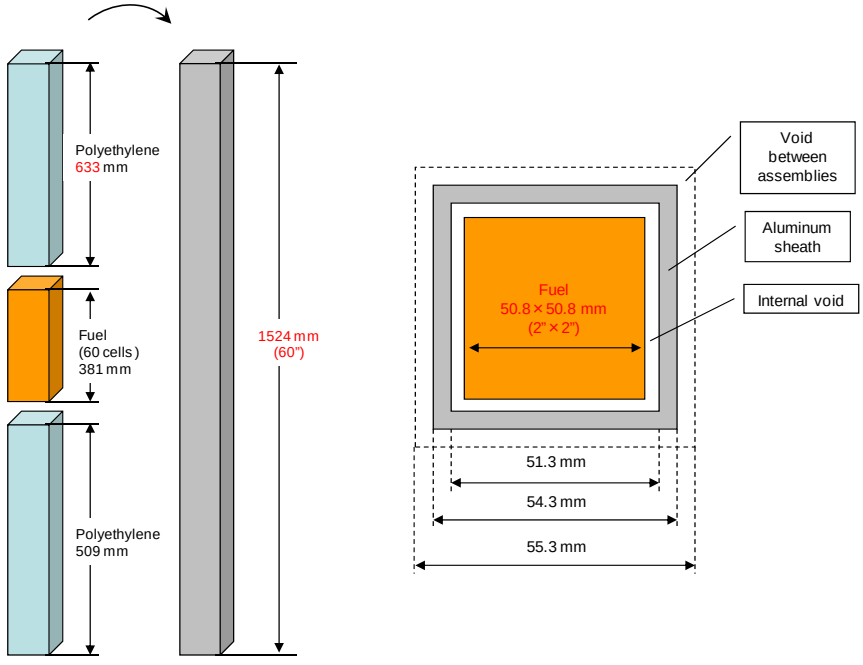

Fig. 1-2 Description of fuel assembly at KUCA

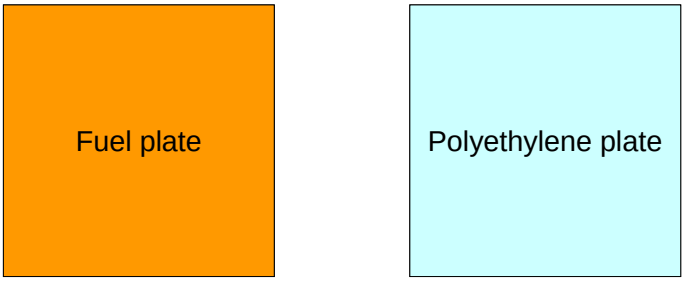

Fig. 1-3 Description of fuel (HEU; 2”×2”) and polyethylene plates (2”×2”)

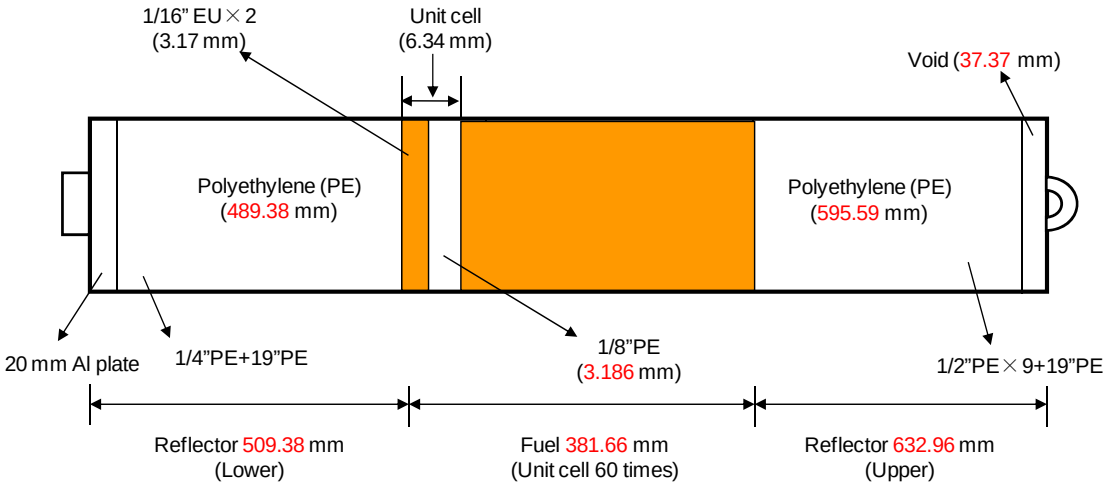

Fig. 1-4 Fall sideways view of fuel assembly “F” shown in Fig. 1-1

1/8”PE = 3.186 mm
1/4”PE = 6.300 mm
1/2”PE = 12.500 mm
19”PE = 483.085 mm

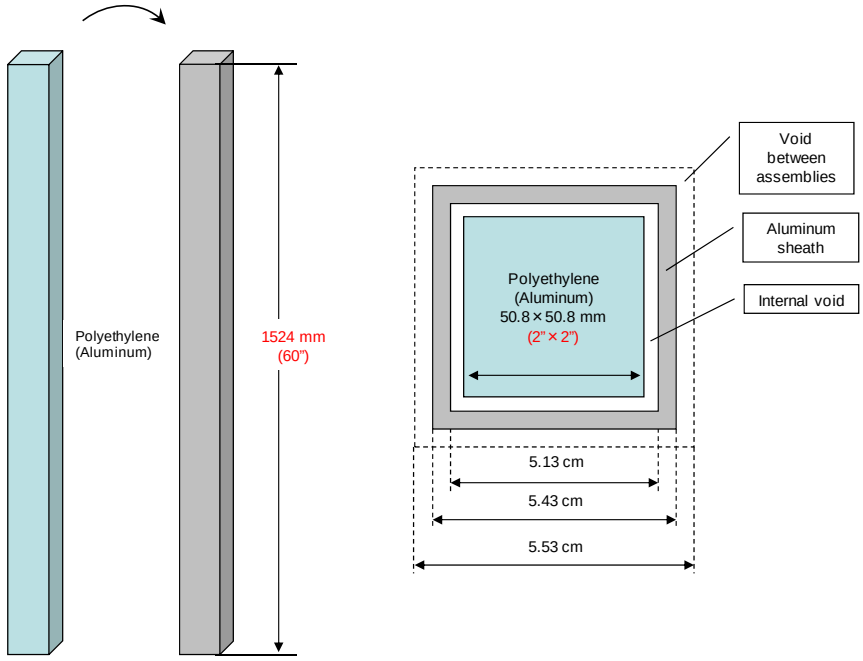

Fig. 1-5 Description of polyethylene reflector at KUCA

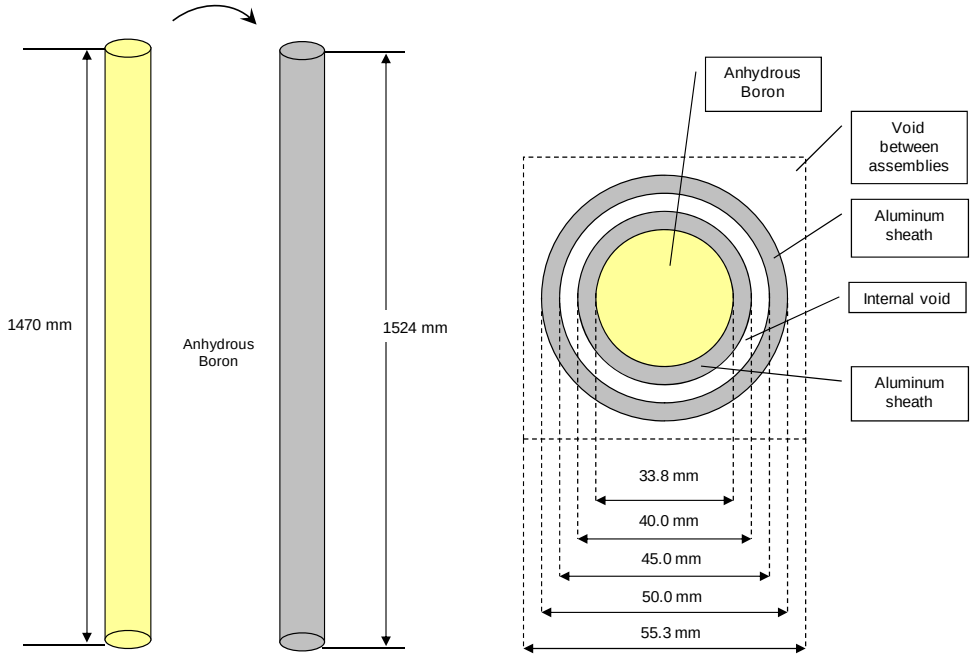

Fig. 1-6 Description of control (safety) rod at KUCA

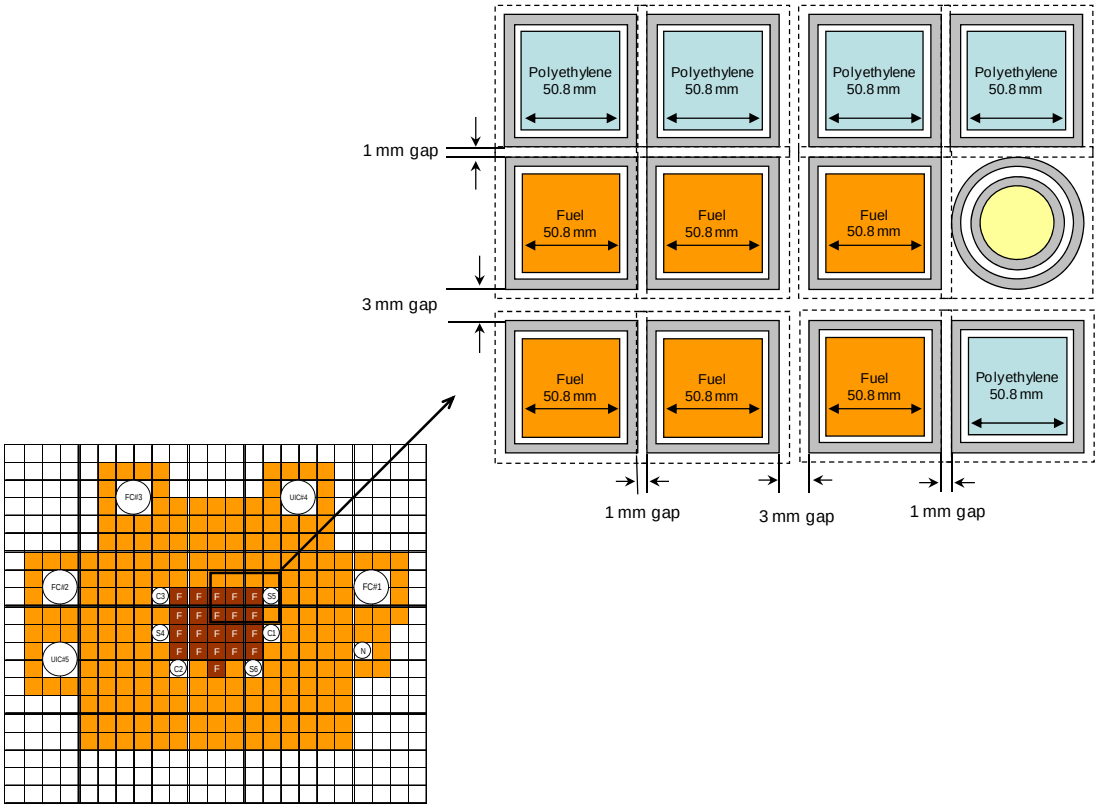

Fig. 1-7 Description of fuel assembly, polyethylene reflector and control rod at KUCA

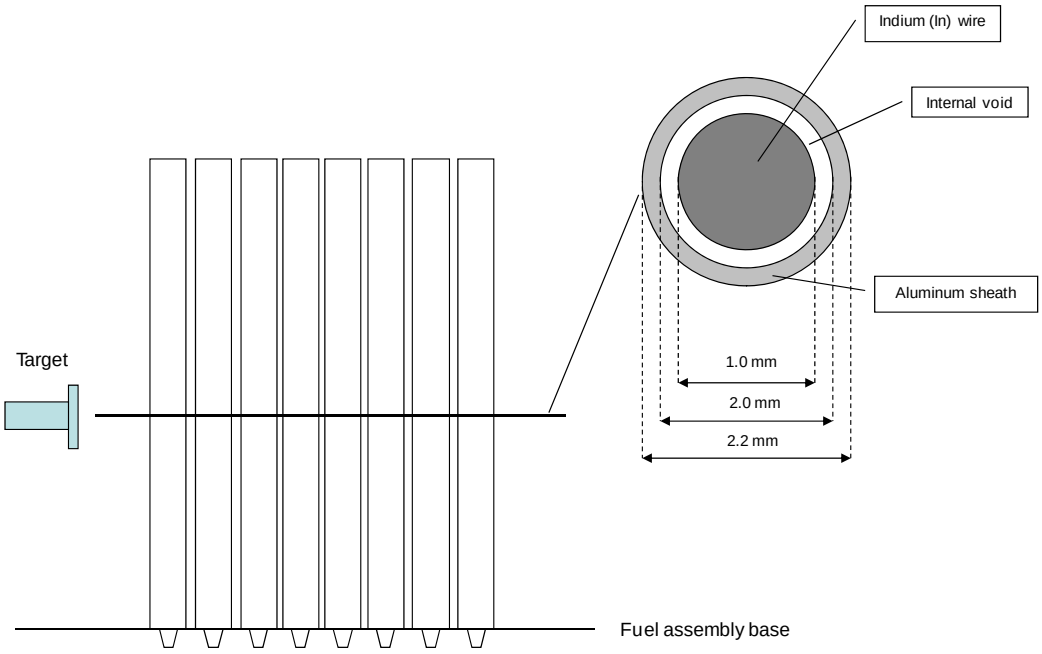

Fig. 1-8 Setting of Indium (In) wire

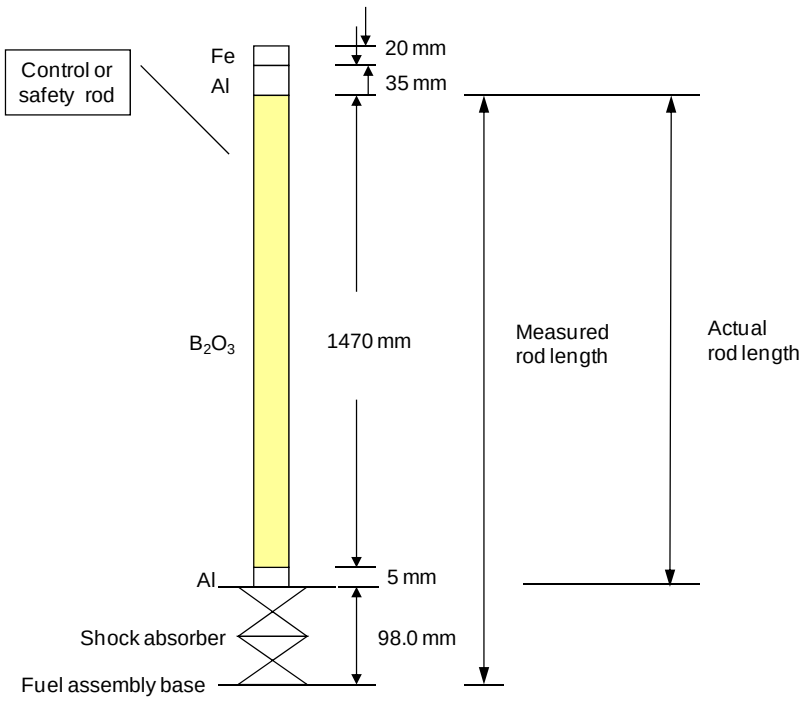

Fig. 1-9 Actual position of control (safety) rod
(Actual position = Measured position – 97.5 mm)

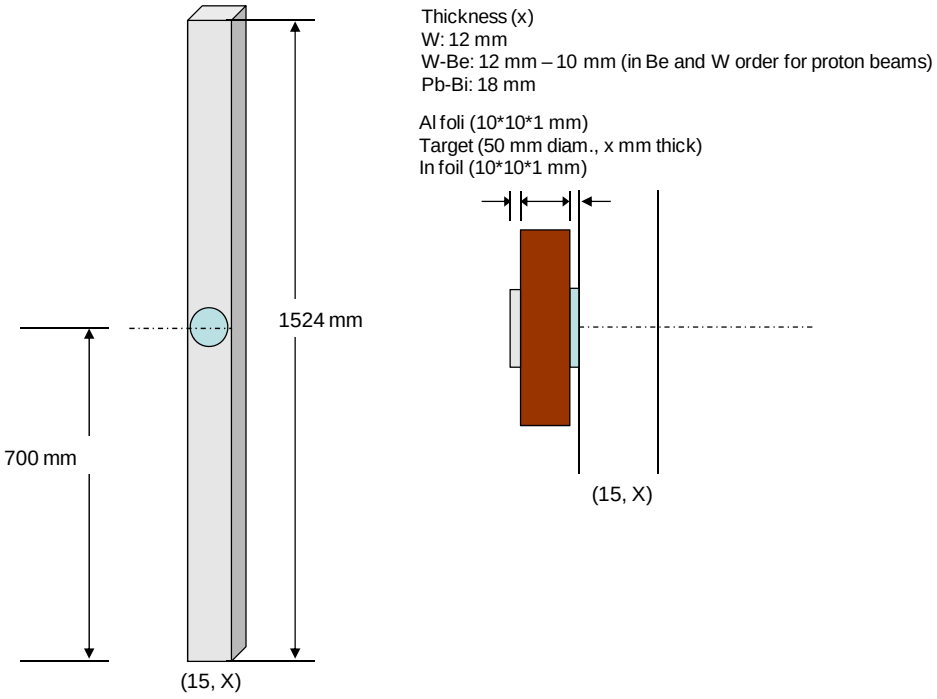

Fig. 1-10 Attachment of target, Al and In foils at the location of core target

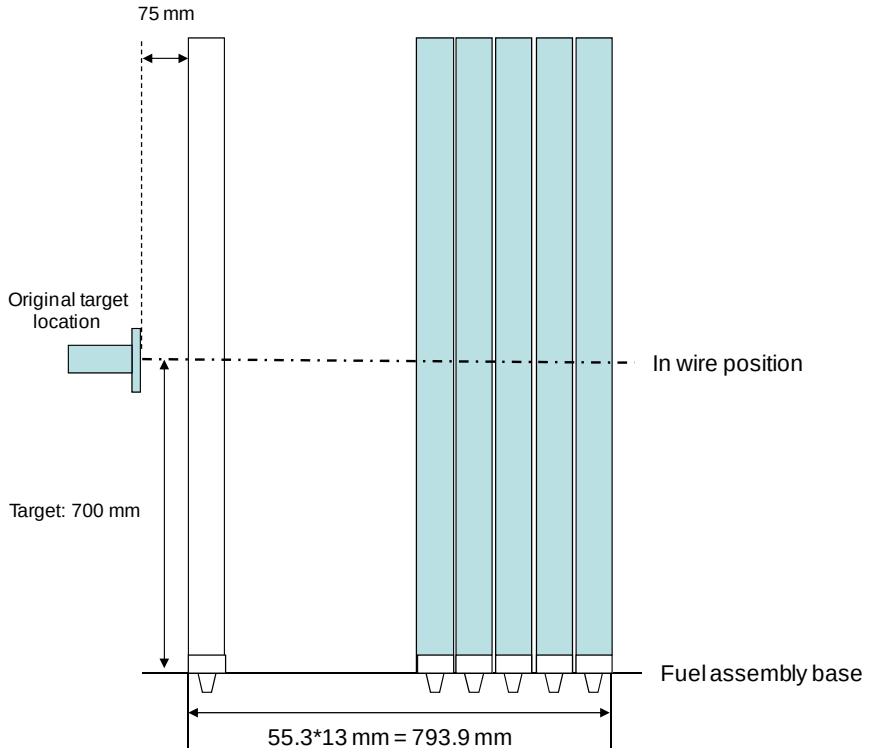

Fig. 1-11 Side view of target and core configuration with 100 MeV protons

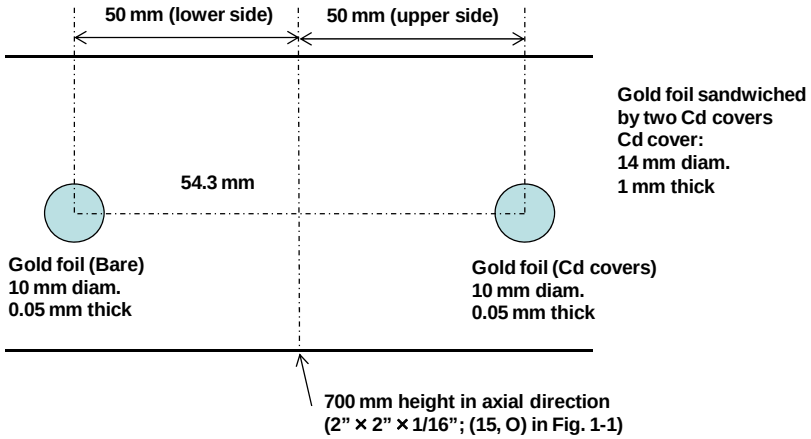

Fig. 1-12 Fall sideways view of HEU fuel rod in (15, O; Fig. 1-1)

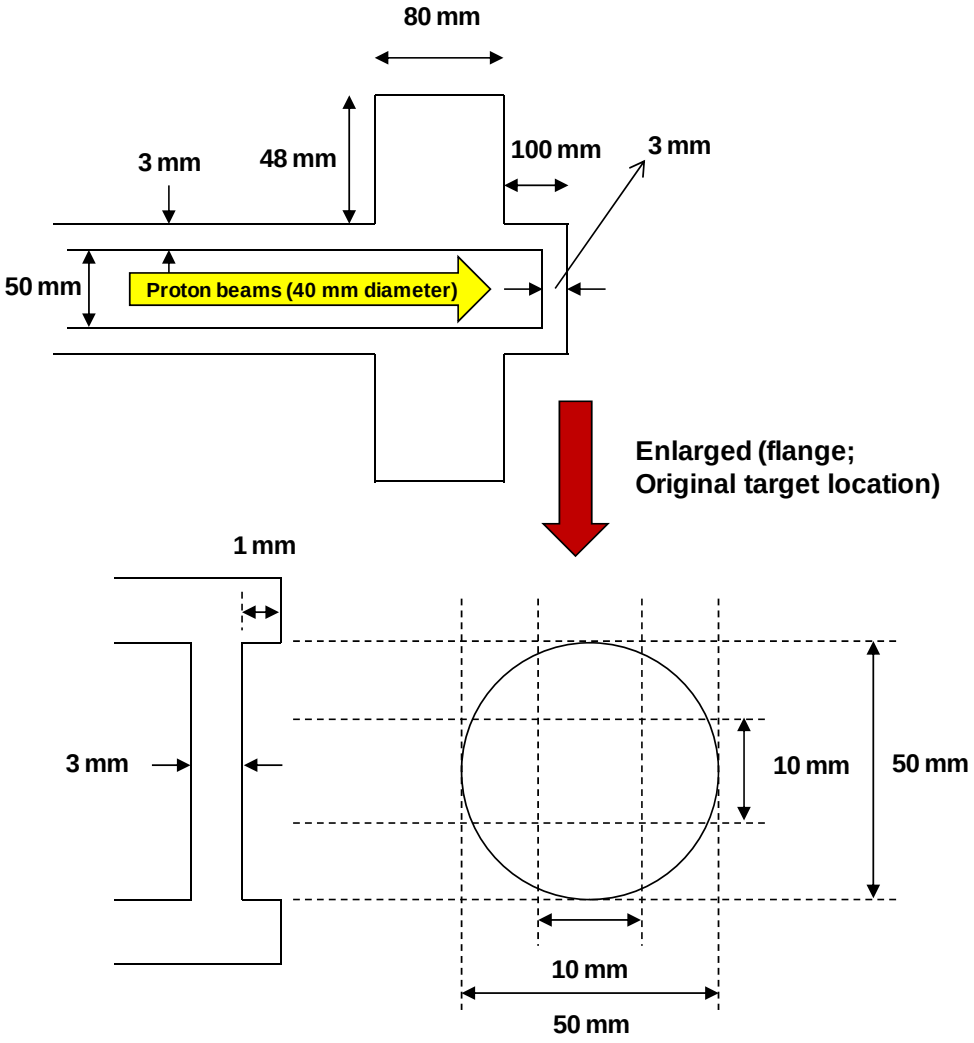

Fig. 1-13 Target configuration of the location of original target

Table 1-1 Atomic densities of 1/16” thick highly-enriched uranium (HEU) fuel plate (U-Al alloy)

Isotope	Atomic density [$\times 10^{24}$/cm^3]
^{234}U	1.13659E-05
^{235}U	1.50682E-03
^{236}U	4.82971E-06
^{238}U	9.25879E-05
Al	5.56436E-02

Table 1-2 Atomic densities of polyethylene (PE) reflector

Isotope	Atomic density [$\times 10^{24}$/cm^3]			
	1/2” thick plate	1/4” thick plate	1/8” thick plate	19” Polyethylene square rod
H	8.06560E-02	8.08711E-02	8.02167E-02	8.00083E-02
C	4.03280E-02	4.04356E-02	4.01084E-02	4.00042E-02

Table 1-3 Atomic densities of control and safety rods

Isotope	Atomic density [$\times 10^{24}$/cm^3]
^{10}B	3.87448E-03
^{11}B	1.68447E-02
^{16}O	3.10787E-02

Table 1-4 Atomic density of aluminum sheath for the core element

Isotope	Atomic density [$\times 10^{24}$/cm^3]
Al	6.00385E-02

Table 1-5 Atomic densities of Cd, In and Au

Foil (wire)	Isotope	Abundance (%)	Purity (%)	Atomic density [$\times 10^{24}$/cm^3]
Cd	^{106}Cd	1.25	99.99	5.39648E-04
	^{108}Cd	0.89	99.99	3.91477E-04
	^{110}Cd	12.51	99.99	5.59564E-03
	^{111}Cd	12.81	99.99	5.78677E-02
	^{112}Cd	24.13	99.99	1.10072E-02
	^{113}Cd	12.22	99.99	5.62419E-03
	^{114}Cd	28.72	99.99	1.33398E-02
	^{116}Cd	7.47	99.99	3.53884E-03
In	^{113}In	4.29	99.99	1.64406E-03
	^{115}In	95.71	99.99	3.66790E-02
Au	^{197}Au	100	99.95	5.90403E-02

Table 1-6 Atomic densities of W, Be and Pb-Bi

Target	Isotope	Abundance (%)	Atomic density [$\times 10^{24}/cm^3$]
W	^{180}W	0.12	8.04702E-05
	^{182}W	26.50	1.64613E-02
	^{183}W	14.31	9.00328E-03
	^{184}W	30.64	1.93829E-02
	^{186}W	28.43	1.81807E-02
Be	^{9}Be	100	1.23487E-01
Pb-Bi (44.5/55.5)	^{204}Pb	1.4	1.87461E-04
	^{206}Pb	24.1	3.25860E-03
	^{207}Pb	22.1	3.00266E-03
	^{208}Pb	52.4	7.15378E-03
	^{209}Bi	100	1.67670E-02

Table 1-7 Dimension of target

Target	Diameter [mm]	Thickness [mm]
W	50.0	12.0
W-Be	50.0	W: 12.0 Be: 10.0
Pb-Bi	50.0	18.0

Table 1-8 Atomic densities of beam tube component (SUS304) shown in Fig. 1-13

Isotope	Atomic density [$\times 10^{24}$/cm^3]
^{54}Fe	3.55712E-03
^{56}Fe	5.58391E-02
^{57}Fe	1.28957E-03
^{58}Fe	1.71618E-04
^{50}Cr	7.51530E-04
^{52}Cr	1.44925E-02
^{53}Cr	1.64333E-03
^{54}Cr	4.09060E-04
^{58}Ni	5.10587E-03
^{60}Ni	1.96674E-03
^{61}Ni	8.54932E-05
^{62}Ni	2.72597E-04
^{64}Ni	6.94130E-05

2. Core Configurations

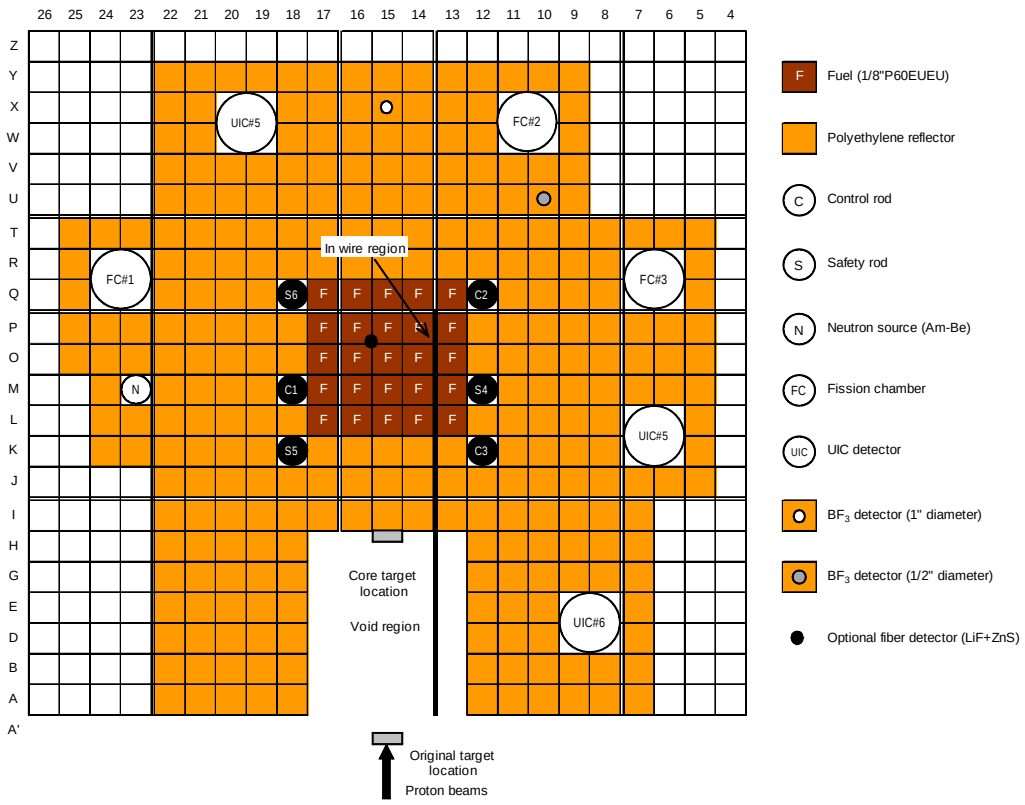

Fig. 2-1 Core configuration of ADS with 100 MeV protons (Black: Full-in; White: Full-out) (in case of the In wire reaction rate distribution)

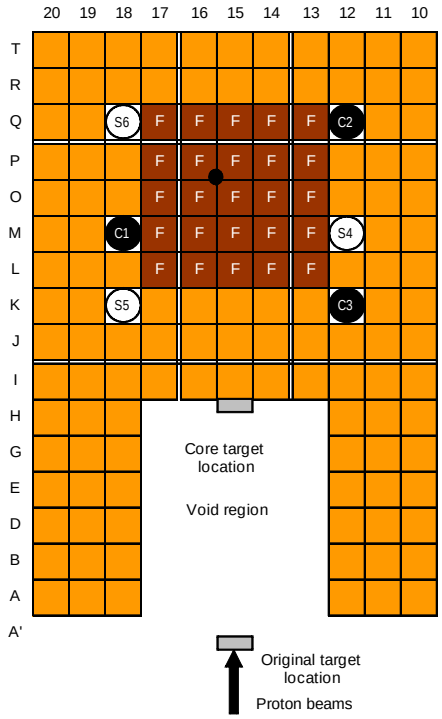

(a) Case I-1

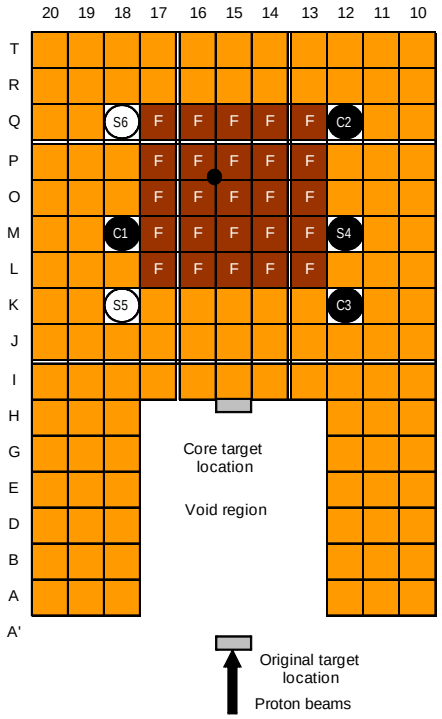

(b) Case I-2

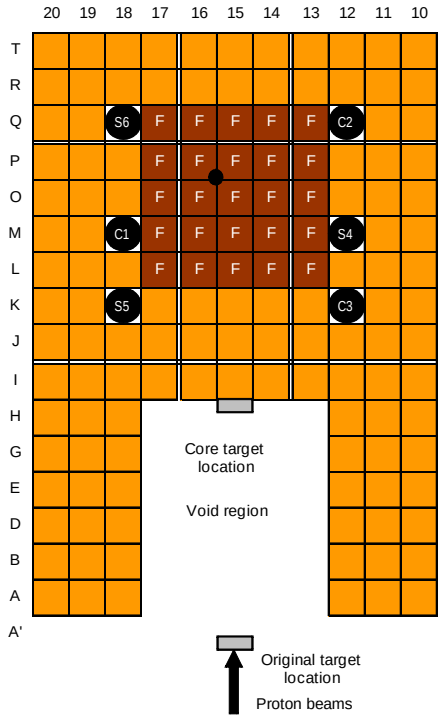

(c) Case I-3

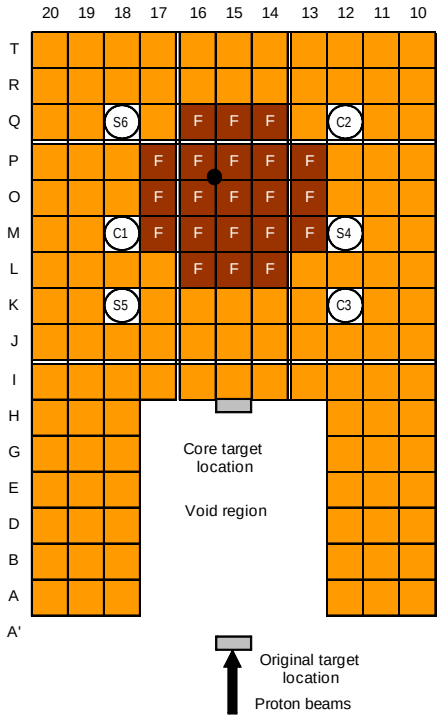

(d) Case I-4

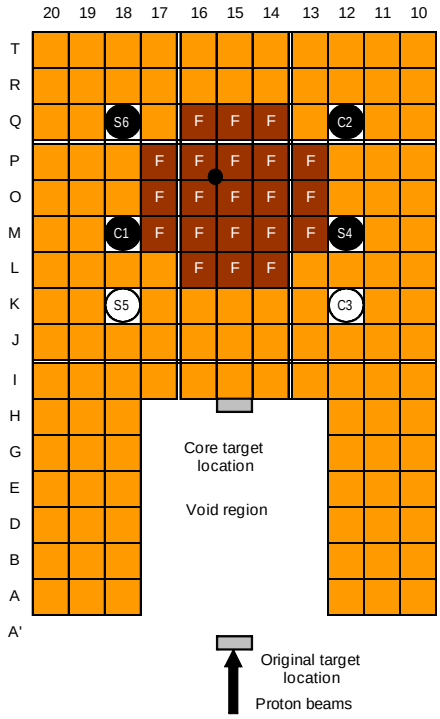

(e) Case I-5

Fig. 2-2 Core configurations of ADS with 100 MeV protons (Black: Full-in; White: Full-out) (in cases of subcriticality measurement by the PNS and the Noise methods)

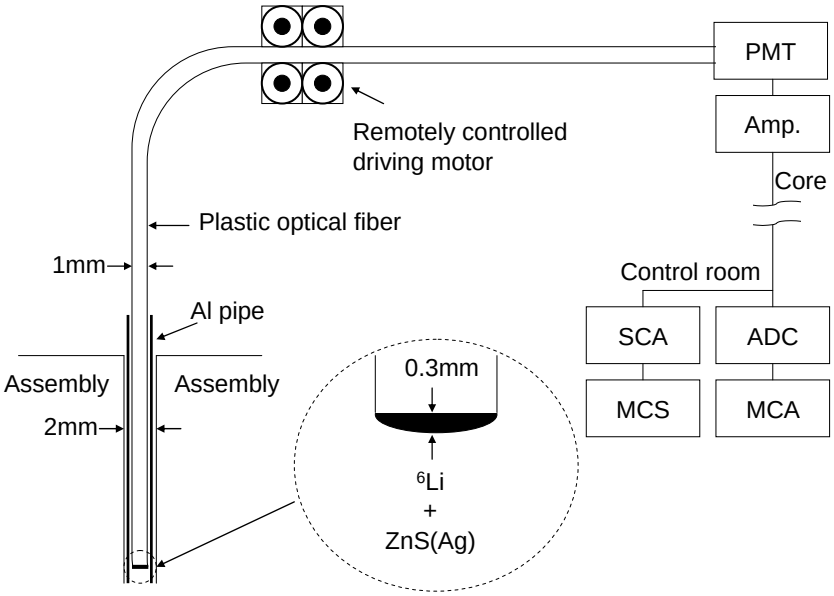

Fig. 2-3 Schema of an optical fiber detection system (Ref. [21])

3. Results of Experiments

3-1. Indium Reaction Rate Distribution

Table 3-1 Control rod positions at the critical state

Rod	Rod position [mm]
C1	676.92
C2	1201.16
C3	1201.43
S4	1200.00
S5	1200.00
S6	1200.00
Excess reactivity [pcm]	180

Table 3-2 Control rod worth

Rod	Rod worth [pcm]
C1 (S4)	805
C2 (S6)	596
C3 (S5)	139

Table 3-3 Measured reaction rates [1/cm^3/s] and Cd ratio

	W target	W-Be target	Pb-Bi target
Au foil (Bare)	(3.017 ± 0.734)E+06	(3.330 ± 0.026)E+06	(2.070 ± 0.158)E+06
Au foil (Cd covered)	(2.240 ± 0.546)E+06	(2.406 ± 0.020)E+06	(1.497 ± 0.116)E+06
^{115}In(n, n')^{115m}In	(2.176 ± 0.078)E+05	(1.777 ± 0.015)E+05	(1.578 ± 0.051)E+05
^{27}Al(n, n+3p)^{24}Na	(1.036 ± 0.062)E+06	(1.185 ± 0.080)E+06	(0.928 ± 0.062)E+06
Cd ratio	1.35 ± 0.27	1.39 ± 0.02	1.38 ± 0.28

Table 3-4 Core condition of indium reaction rate distribution in subcritical state

Case	Number of fuel rods	Rod insertion
Case I-3 (refer to Table 3-6)	25	C1, C2, C3, S4, S5, S6

Table 3-5 Specification of measurement of reaction rate distribution

Reaction	Location	Foil/Wire
^{115}In(n, n')^{115m}In	Target (refer to Fig. 1-10)	10*10*1 mm
^{115}In(n, γ)^{116}In	Core (refer to Fig. 1-11)	1 mm diameter, 800 mm long

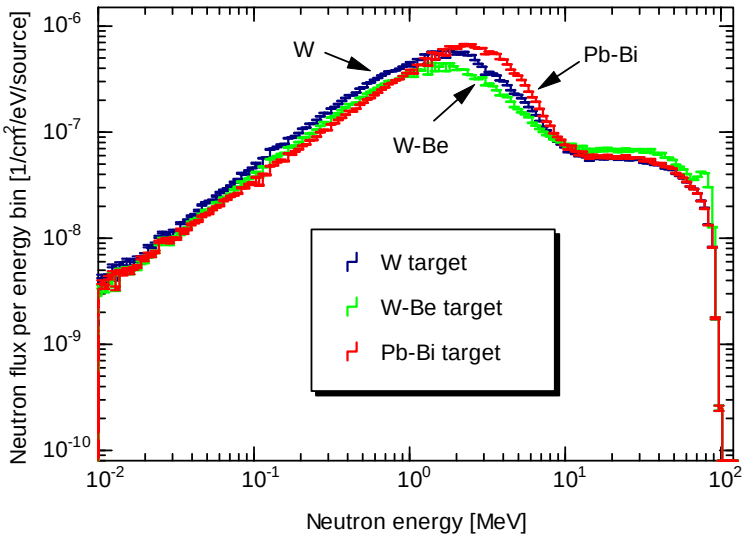

Fig. 3-1 Comparison between neutron spectra with the use of W, W-Be and Pb-Bi targets

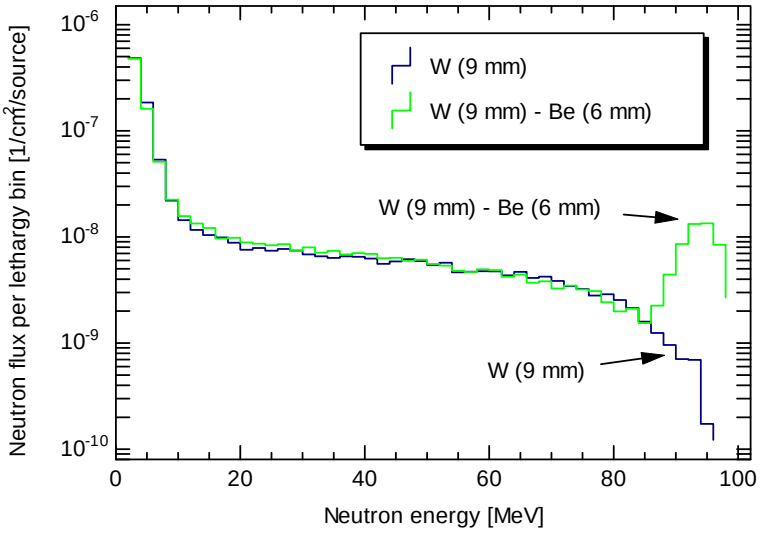

Fig. 3-2 Comparison between neutron spectra with the use of W and W-Be targets

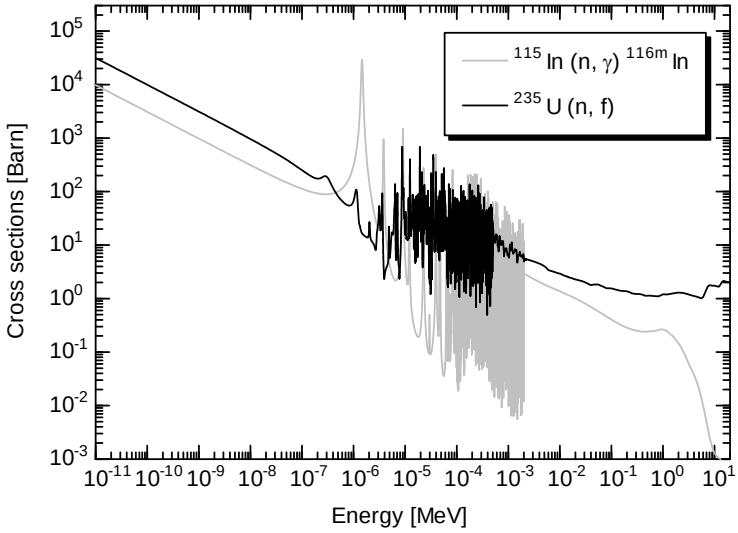

Fig. 3-3 Proportionality of cross sections of ^{115}In capture and ^{235}U fission reactions

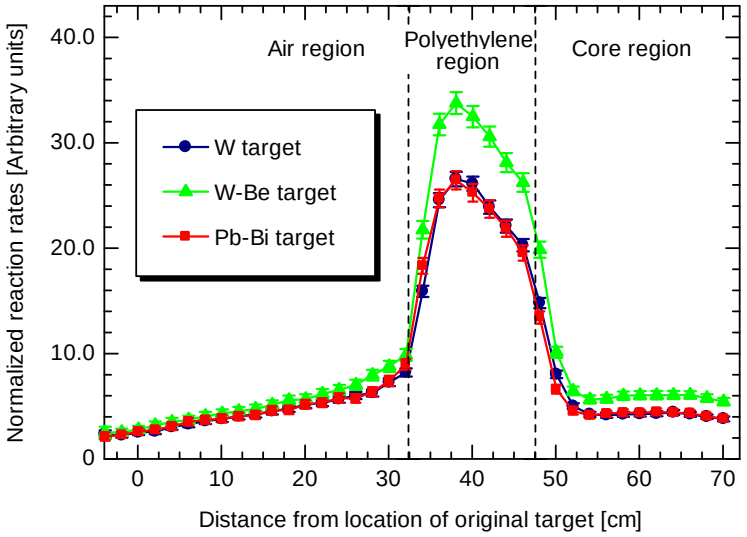

Fig. 3-4 Comparison between normalized reaction rates obtained in ADS experiments

3-2. Time evolution data of PNS and Noise methods

Table 3-6 List of core condition in all the cores shown in Fig. 2-2

Case	Number of fuel rods	Rod insertion	100 MeV protons	
			PNS method	Noise method
Case I-1	25	C1, C2, C3	Available	Available
Case I-2	25	C1, C2, C3, S4	Available	Available
Case I-3	25	C1, C2, C3, S4, S5, S6	Available	Available
Case I-4	21	All six rods withdrawn	Available	Available
Case I-5	21	C1, C2, S4, S6	Available	Available

*: PNS method: Pulsed neutron source method; Noise method: Feynman-α method

Note that subcriticalities in Cases I-1, I-2 and I-3 were deduced by the excess reactivity and the control rod worth in Tables 3-2 and 3-3. In Cases I-4 and I-5, the subcriticality was deduced with the use of calculation results.

Table 3-7 Time evolution data on the PNS and Noise methods

Case	100 MeV protons	
	Repetition [Hz]	Width [ns]
Case I-1	20	100
Case I-2	20	100
Case I-3	20	100
Case I-4	20	100
Case I-5	20	100

*: Proton beam intensity was 1 nA; Spot size of proton beams: 40 mm.

Table 3-8 Measured prompt neutron decay constants α [1/s] deduced by least-squared fitting in the PNS method

	Neutron decay constants α [1/s]		
Target	BF_3 #1 in (10, U)	BF_3 #2 in (15, X)	Optical fiber
	Case I-1		
W	737.1 ± 56.0	739.6 ± 9.5	706.4 ± 83.3
W-Be	732.5 ± 5.2	747.8 ± 5.5	782.0 ± 5.1
Pb-Bi	737.7 ± 10.9	731.9 ± 10.6	756.5 ± 12.5
	Case I-2		
W	1059.9 ± 10.0	1075.0 ± 5.8	1215.2 ± 12.5
W-Be	1062.7 ± 10.0	1085.6 ± 4.0	1101.9 ± 5.3
Pb-Bi	1070.1 ± 21.5	1072.0 ± 20.0	1080.8 ± 8.3
	Case I-3		
W	1364.2 ± 8.4	1372.5 ± 9.9	1379.6 ± 68.4
W-Be	1377.2 ± 6.5	1383.2 ± 6.8	1402.3 ± 10.3
Pb-Bi	1338.0 ± 3.7	1358.3 ± 4.0	1381.5 ± 7.1
	Case I-4		
W	1052.0 ± 7.5	1033.3 ± 8.8	1204.5 ± 16.6
W-Be	1033.2 ± 3.1	1027.7 ± 3.5	1073.8 ± 4.1
Pb-Bi	1006.3 ± 5.6	1004.1 ± 6.1	1083.2 ± 5.3
	Case I-5		
W	1844.6 ± 21.3	1845.9 ± 17.7	1922.5 ± 33.3
W-Be	1770.5 ± 3.7	1697.0 ± 4.6	1909.1 ± 3.9
Pb-Bi	1785.2 ± 9.4	1742.1 ± 8.7	1895.5 ± 11.1

Table 3-9 Measured subcriticality [pcm] deduced by the extrapolated area ratio method

	Subcriticality ρ [pcm] (by Area ratio method)		
Target	BF_3 #1 in (10, U)	BF_3 #2 in (15, X)	Optical fiber
	Case I-1 (Reference: ρ_{exp} = 1360 pcm)		
W	1132 ± 17	1393 ± 20	1888 ± 27
W-Be	1145 ± 18	1458 ± 21	1473 ± 21
Pb-Bi	1166 ± 18	1387 ± 20	1390 ± 20
	Case I-2 (Reference: ρ_{exp} = 2165 pcm)		
W	1877 ± 27	2363 ± 35	3002 ± 44
W-Be	1879 ± 28	2463 ± 36	2229 ± 33
Pb-Bi	1926 ± 29	2356 ± 35	2252 ± 33
	Case I-3 (Reference: ρ_{exp} = 2900 pcm)		
W	2398 ± 35	3156 ± 46	3822 ± 58
W-Be	2502 ± 39	3405 ± 51	2939 ± 45
Pb-Bi	2624 ± 39	3238 ± 48	2977 ± 45
	Case I-4 (Reference: ρ_{MCNPX} = 2773 pcm)		
W	2682 ± 39	3291 ± 48	3672 ± 55
W-Be	2688 ± 41	3483 ± 52	2910 ± 43
Pb-Bi	2738 ± 41	3302 ± 49	2922 ± 44
	Case I-5 (Reference: ρ_{MCNPX} = 4902 pcm)		
W	4944 ± 78	6386 ± 101	6228 ± 99
W-Be	5004 ± 83	7050 ± 114	4929 ± 77
Pb-Bi	4903 ± 77	6356 ± 92	4912 ± 74

(β_{eff} = 807 pcm; Λ = 3.050E-05 s)

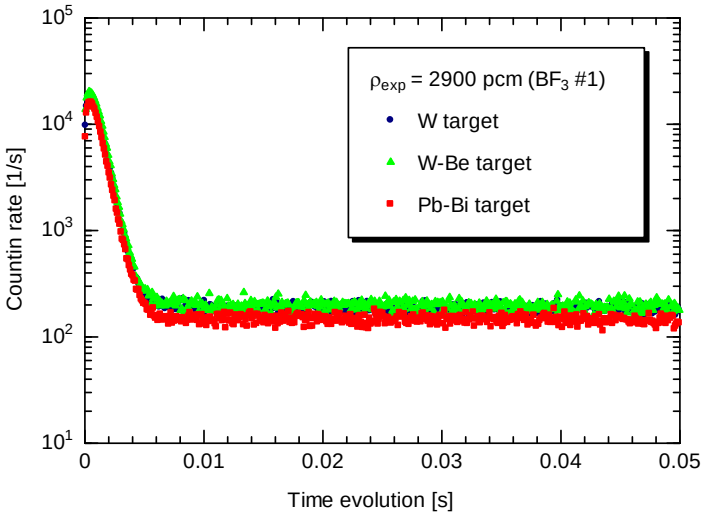

Fig. 3-5 Experimental results of time evolution on prompt and delayed neutron behaviors at position (10, U) of BF_3 detector #1 in Case I-3

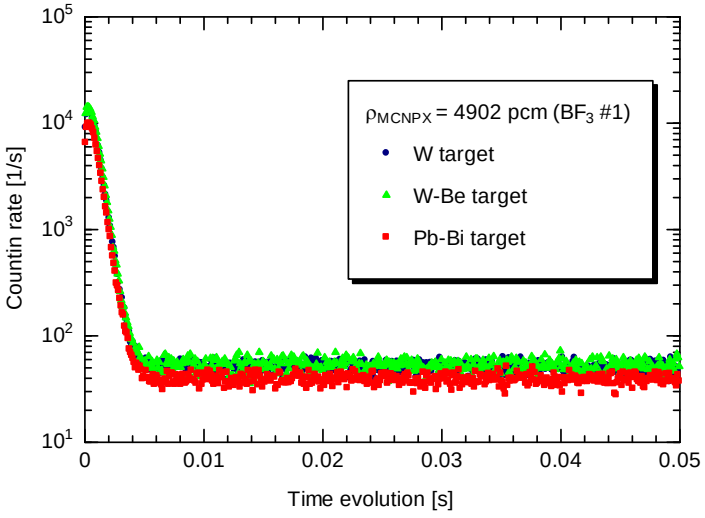

Fig. 3-6 Experimental results of time evolution on prompt and delayed neutron behaviors at position (10, U) of BF_3 detector #1 in Case I-5

Table 3-10 Measured prompt neutron decay constants α [1/s] deduced by least-squared fitting in the Noise method

	Neutron decay constants α [1/s]		
Target	BF_3 #1 in (10, U)	BF_3 #2 in (15, X)	Optical fiber
	Case I-1		
W	632.5 ± 7.1	665.4 ± 12.5	636.6 ± 10.8
W-Be	641.8 ± 21.2	683.0 ± 13.5	705.6 ± 11.8
Pb-Bi	616.2 ± 30.4	650.7 ± 26.8	714.2 ± 19.4
	Case I-2		
W	878.7 ± 22.2	869.1 ± 28.2	1089.8 ± 60.2
W-Be	874.7 ± 12.6	912.8 ± 23.7	1073.4 ± 60.4
Pb-Bi	885.0 ± 25.3	898.5 ± 36.3	970.2 ± 62.6
	Case I-3		
W	1086.4 ± 21.6	1103.1 ± 26.8	1407.5 ± 57.1
W-Be	1094.3 ± 11.8	1159.6 ± 16.4	1296.0 ± 18.6
Pb-Bi	1124.8 ± 13.9	1132.8 ± 23.4	1308.5 ± 19.5
	Case I-4		
W	889.0 ± 11.6	941.8 ± 20.5	1072.8 ± 23.8
W-Be	880.1 ± 12.8	975.5 ± 35.0	999.7 ± 11.4
Pb-Bi	900.0 ± 17.5	931.1 ± 10.5	1021.5 ± 23.3
	Case I-5		
W	1487.9 ± 48.9	1451.6 ± 35.4	1965.8 ± 91.7
W-Be	1456.5 ± 18.8	1575.3 ± 28.5	1746.6 ± 23.2
Pb-Bi	1390.4 ± 95.4	1431.6 ± 96.1	1682.6 ± 142.9

Table 3-11 Measured subcriticality [pcm] deduced by the Noise method

	Subcriticality ρ [pcm] (by Feynman-α method)		
Target	BF_3 #1 in (10, U)	BF_3 #2 in (15, X)	Optical fiber
	Case I-1 (Reference: ρ_{exp} = 1360 pcm)		
W	1122 ± 25	1515 ± 40	1406 ± 35
W-Be	1151 ± 66	1581 ± 43	1667 ± 38
Pb-Bi	1073 ± 94	1459 ± 83	1699 ± 61
	Case I-2 (Reference: ρ_{exp} = 2165 pcm)		
W	1873 ± 69	2285 ± 87	3119 ± 184
W-Be	1861 ± 41	2450 ± 74	3057 ± 185
Pb-Bi	1892 ± 78	2396± 112	2667 ± 191
	Case I-3 (Reference: ρ_{exp} = 2900 pcm)		
W	2507 ± 67	3169 ± 83	4320 ± 175
W-Be	2531 ± 39	3383 ± 52	3898 ± 59
Pb-Bi	2624 ± 45	3282 ± 73	3946 ± 61
	Case I-4 (Reference: ρ_{MCNPX} = 2773 pcm)		
W	1905 ± 38	2560 ± 64	3055 ± 74
W-Be	1877 ± 41	2884 ± 108	2778 ± 37
Pb-Bi	1938 ± 55	2519 ± 35	2861 ± 72
	Case I-5 (Reference: ρ_{MCNPX} = 4902 pcm)		
W	3731 ± 150	4486 ± 109	6430 ± 280
W-Be	3634 ± 60	4954 ± 86	5601 ± 73
Pb-Bi	3434 ± 291	4411 ± 294	5360 ± 436

(β_{eff} = 807 pcm; Λ = 3.050E-05 s)

Phase II

Study on Subcriticality Measurements

Appendix-II

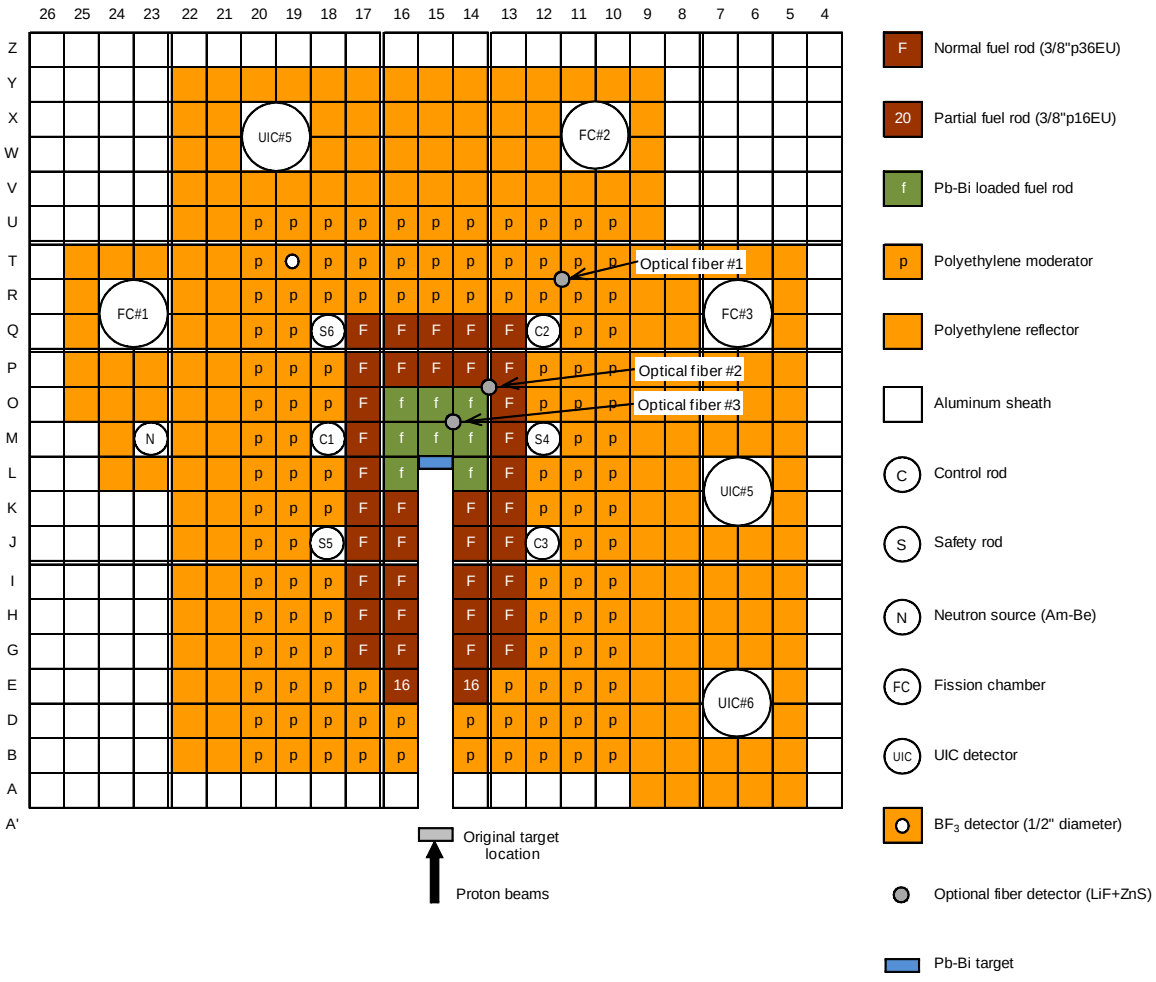

Fig. 4-1 Core configuration of ADS with 100 MeV protons (Black: Full-in; White: Full-out)
(in case of the subcriticality measurements)

***Notification**:

1. Please refer to Table 1-7 and Fig. 1-10, concerning atomic density of the Pb-Bi target.
2. In this Phase II, new polyethylene moderator "p" (small letter: "polyethylene moderator") was installed in the core as shown in Table 4-1. Please make sure of difference between the polyethylene "moderator" and "reflector (Table 1-2)."

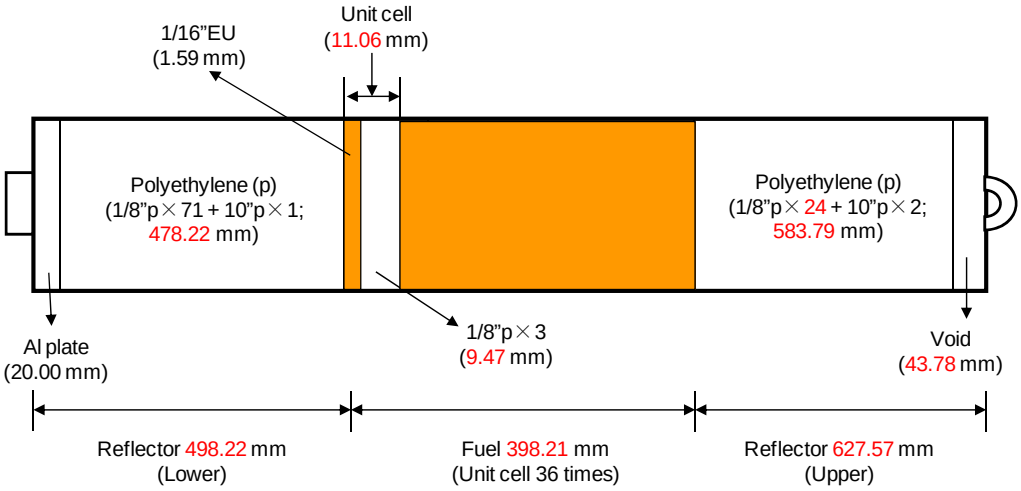

Fig. 4-2 Fall sideways view of fuel assembly “F” shown in Fig. 4-1
(F: 3/8”p36EU)

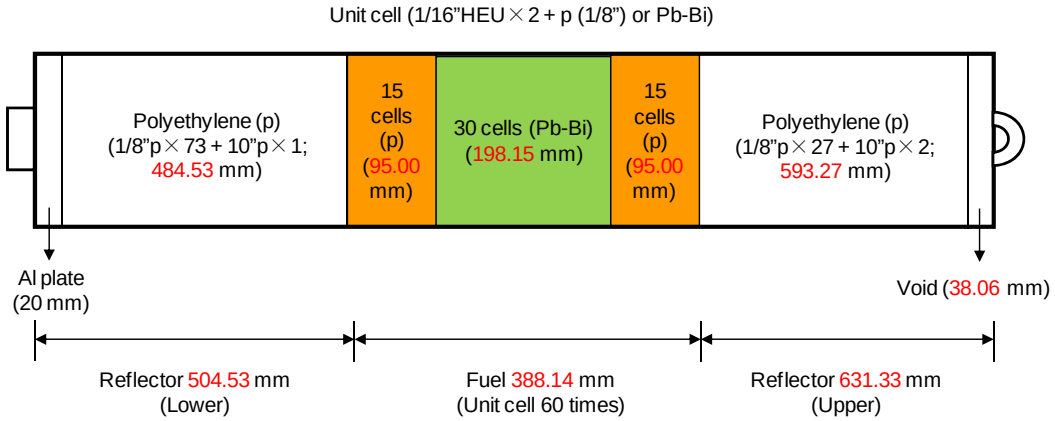

Fig. 4-3 Fall sideways view of fuel assembly “f” shown in Fig. 4-1
(f: 1/8”p15EUEU < 1/8”PbBi30EUEU >1/8”p15EUEU)

1/8”p = 3.158 mm

10”p = 254.000 mm

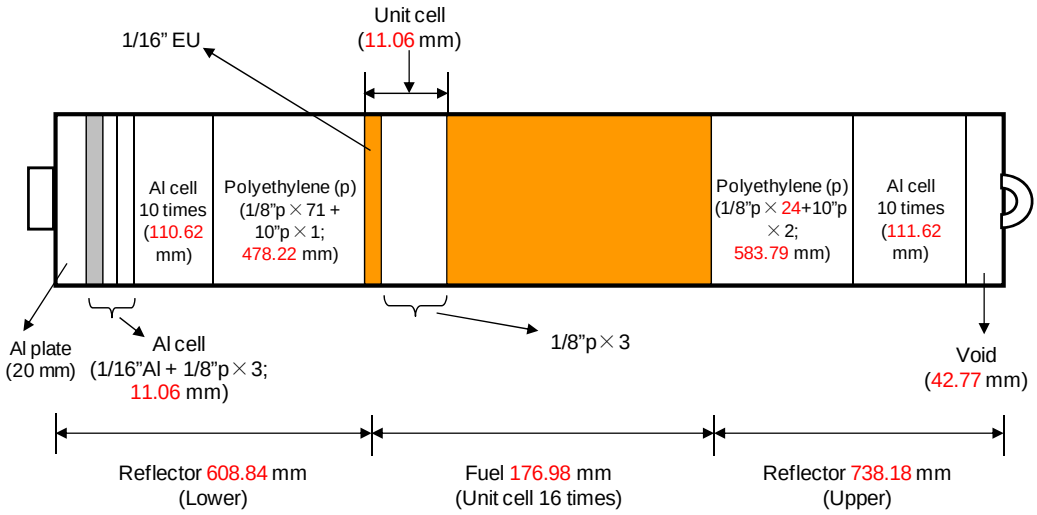

Fig. 4-4 Fall sideways view of fuel assembly "16" shown in Fig. 4-1
(16: 3/8"p16EU)

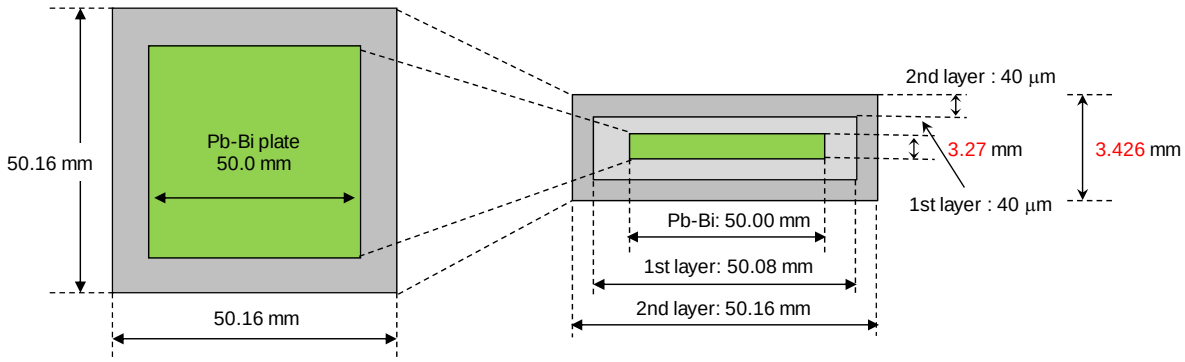

Fig. 4-5 Description of Pb-Bi plate covering over coating materials shown in Fig. 4-3

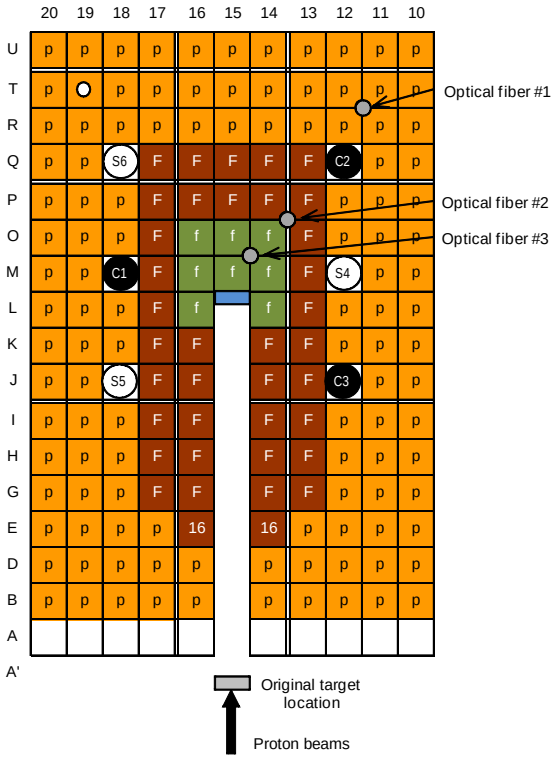

(a) Case II-1

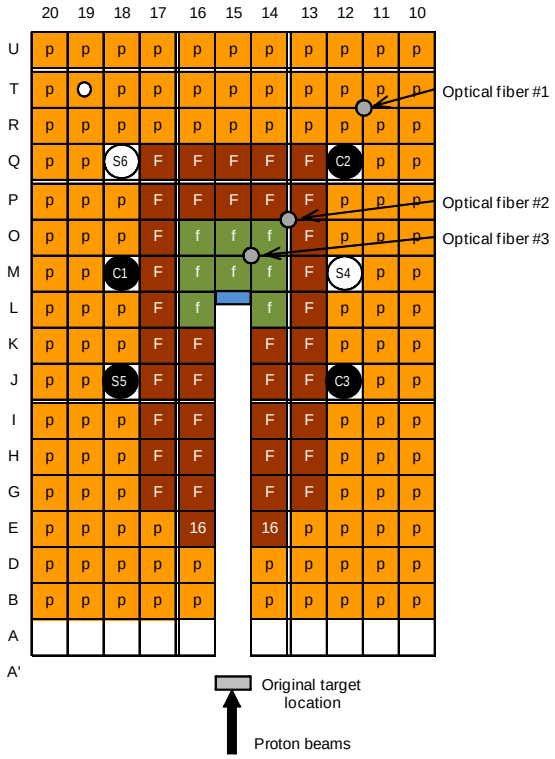

(b) Case II-2

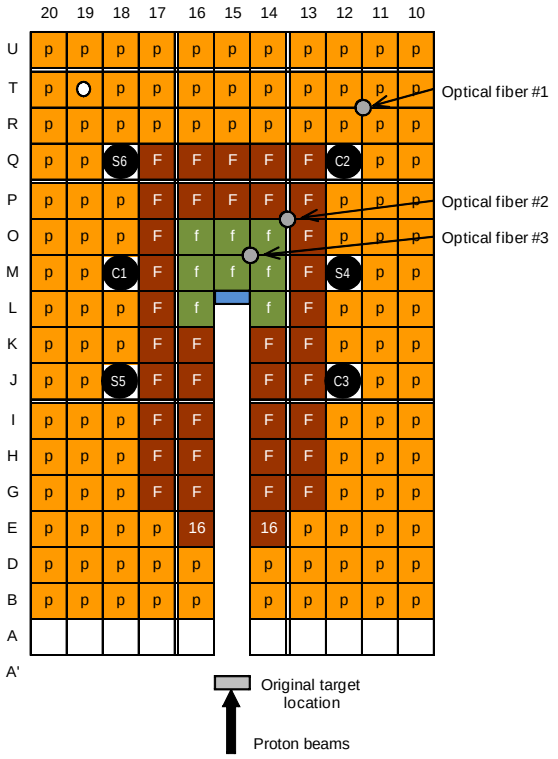

(c) Case II-3

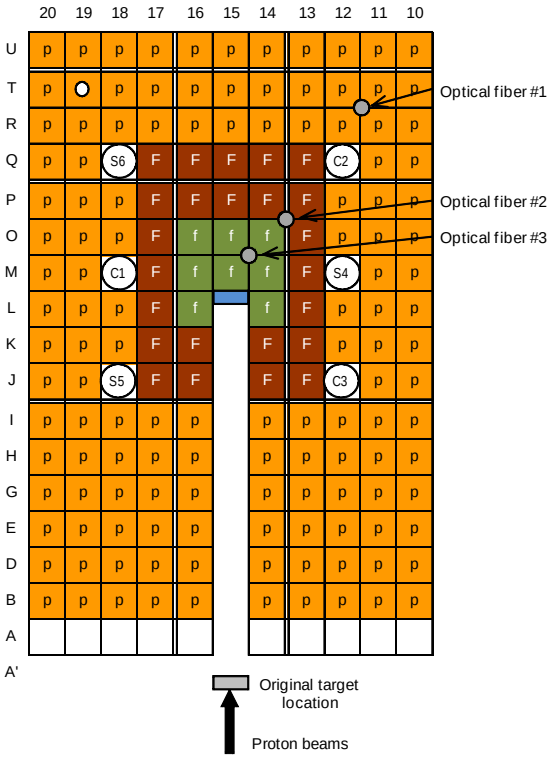

(d) Case II-4

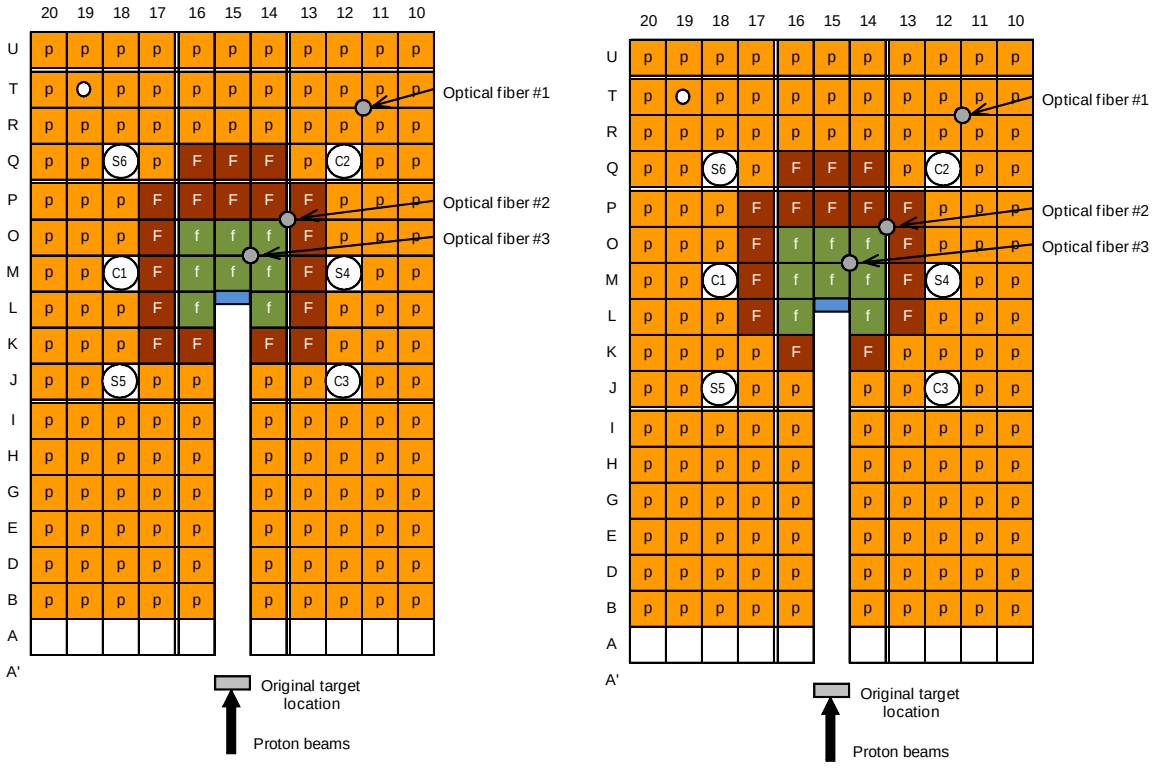

(e) Case II-5 (f) Case II-6

Fig. 4-6 Core configurations of ADS with 100 MeV protons (Black: Full-in; White: Full-out) (in cases of subcriticality measurement by the PNS and the Noise methods)

Table 4-1 Atomic density of polyethylene moderator "p" shown in Figs. 4-1 through 4-4

Isotope	Atomic density [$\times 10^{24}/cm^3$]	
	1/8" thick plate	10" Polyethylene square rod
H	7.77938E-02	7.97990E-02
C	3.95860E-02	4.08960E-02

Table 4-2 Number density of coating materials (Face; 1st and Base 2nd layers) over Pb-Bi plate

Nuclide	Isotope	Atomic density [$\times 10^{24}$/cm^3] (Face; 1st layer)	Atomic density [$\times 10^{24}$/cm^3] (Base; 2nd layer)
H	^{1}H	2.83301E-03	3.78991E-03
	^{2}H	4.25015E-07	5.64072E-07
C	-	2.27058E-03	4.03671E-03
O	^{16}O	2.06885E-03	4.58782E-04
	^{17}O	7.88039E-07	1.74753E-07
	^{18}O	4.14757E-06	9.19753E-07
Ti	^{46}Ti	2.50941E-05	5.36896E-05
	^{47}Ti	2.28983E-05	4.89918E-05
	^{48}Ti	2.31493E-04	4.95287E-04
	^{49}Ti	1.72522E-05	3.69116E-05
	^{50}Ti	1.69385E-05	3.62405E-05
Si	^{28}Si	-	1.86243E-05
	^{29}Si	-	9.43026E-07
	^{30}Si	-	6.25992E-07
S	^{32}S	4.16818E-04	-
	^{33}S	3.28997E-06	-
	^{34}S	1.84677E-05	-
	^{35}S	8.77326E-08	-
Ba	^{132}Ba	4.43050E-07	-
	^{134}Ba	1.06025E-05	-
	^{135}Ba	2.89167E-05	-
	^{136}Ba	3.44526E-05	-
	^{137}Ba	4.92619E-05	-
	^{138}Ba	3.14521E-04	-

4. Results of Experiments

Table 4-3 List of core condition in all the cores shown in Fig. 4-6

Case	Number of fuel rods	Rod insertion	100 MeV protons	
			PNS method	Noise method
Case II-1	46	C1, C2, C3	Available	Available
Case II-2	46	C1, C2, C3, S5	Available	Available
Case II-3	46	C1, C2, C3, S4, S5, S6	Available	Available
Case II-4	32	All six rods withdrawn	Available	Available
Case II-5	26	All six rods withdrawn	Available	Available
Case II-6	24	All six rods withdrawn	Available	Available

*: PNS method: Pulsed neutron source method; Noise method: Feynman-α method

Note that subcriticalities in Cases II-1, II-2 and II-3 were deduced by the excess reactivity and the control rod worth in Tables 4-2 and 4-3. In Cases II-4, II-5 and II-6, the subcriticality was deduced with the use of calculation results.

Table 4-4 Control rod positions at the critical state

Rod	Rod position [mm]
C1	1200.00
C2	525.39
C3	1200.00
S4	1200.00
S5	1200.00
S6	1200.00
Excess reactivity [pcm]	149±3

Table 4-5 Control rod worth

Rod	Rod worth [pcm]
C1 (S4)	549±3
C2 (S6)	194±1
C3 (S5)	483±2

β_{eff} = 781±4 [pcm]

Table 4-6 Effective multiplication factor in Cases II-1 through II-6

Case	k_{eff} (MCNP6.1 with ENDF/B-VII.0)
Critical state	1.00378 ± 0.0004
Case II-1	0.99219 ± 0.0004
Case II-2	0.98723 ± 0.0004
Case II-3	0.97950 ± 0.0004
Case II-4	0.95784 ± 0.0004
Case II-5	0.91355 ± 0.0004
Case II-6	0.90006 ± 0.0004

Table 4-7 Time evolution data on the PNS and Noise methods

Case	100 MeV protons	
	Repetition [Hz]	Width [ns]
Case II-1	20	50
Case II-2	20	50
Case II-3	20	50
Case II-4	20	50
Case II-5	20	50
Case II-6	20	50

*: Proton beam intensity was 1 nA; Spot size of proton beams: 40 mm.

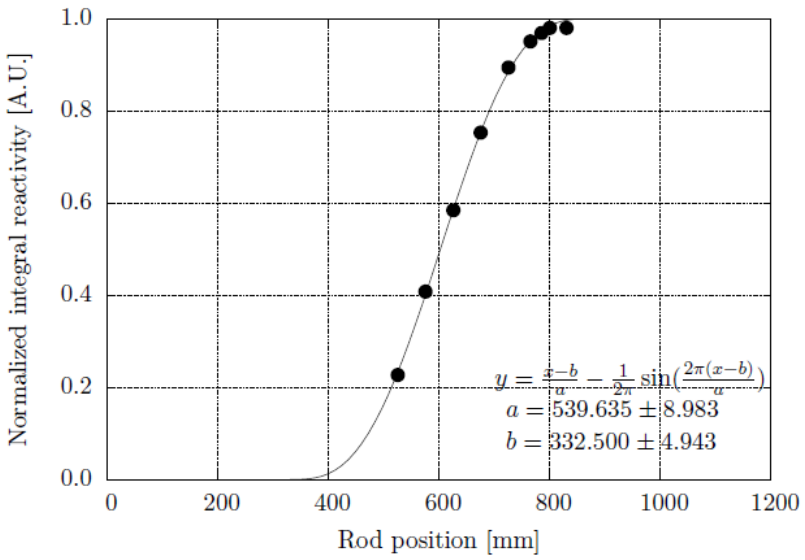

Fig. 4-7 Calibration curve of C2 (as well as in C1 and C3) control rod

4-1 Time evolution data of PNS and Noise methods

Table 4-8 Measured prompt neutron decay constants α [1/s] deduced by least-squared fitting in the PNS method

	Neutron decay constants α [1/s]		
Case	Fiber #1	Fiber #2	Fiber #3
Case II-1	398.0 ± 2.5	326.8 ± 2.7	494.5 ± 10.2
Case II-2	506.7 ± 3.0	452.6 ± 2.8	685.4 ± 10.8
Case II-3	672.6 ± 3.5	631.9 ± 1.8	1019.7 ± 8.3
Case II-4	982.5 ± 4.4	971.3 ± 3.1	1378.0 ± 18.4
Case II-5	1665.4 ± 8.7	1680.7 ± 5.1	1827.7 ± 22.8
Case II-6	1910.9 ± 7.4	1930.7 ± 3.3	2061.0 ± 37.8

Table 4-9 Measured subcriticality [pcm] deduced by the extrapolated area ratio method

			Subcriticality ρ [pcm] (by Area ratio method)		
Case	β_{eff} [pcm]	Reference [pcm]	Fiber #1	Fiber #2	Fiber #3
Case II-1	785 ± 4	ρ_{exp} = 1160 ± 5	1224 ± 10	1153 ± 8	2108 ± 59
Case II-2	785 ± 4	ρ_{exp} = 1684 ± 6	1880 ± 15	1604 ± 11	4490 ± 109
Case II-3	783 ± 5	ρ_{exp} = 2483 ± 6	2824 ± 22	2250 ± 13	10347 ± 116
Case II-4	788 ± 5	ρ_{MCNP} = 4812 ± 6	5656 ± 62	4177 ± 31	22939 ± 1279
Case II-5	816 ± 5	ρ_{MCNP} = 9895 ± 6	12819 ± 137	8187 ± 54	14985 ± 1136
Case II-6	806 ± 5	ρ_{MCNP} = 11556 ± 6	16312 ± 160	9738 ± 64	19109 ± 2563

(β_{eff} : MCNP6.1 with JENDL-4.0)

Table 4-10 Measured prompt neutron decay constants α [1/s] deduced by least-squared fitting in the Noise method

	Neutron decay constants α [1/s]		
Case	Optical fiber #1	Optical fiber #2	Optical fiber #3
Case II-1	400.6 ± 9.2	367.1 ± 5.8	554.0 ± 16.8
Case II-2	498.1 ± 4.6	463.5 ± 4.0	700.0 ± 6.7
Case II-3	654.5 ± 2.4	620.0 ± 1.8	877.3 ± 4.8
Case II-4	814.6 ± 5.8	822.0 ± 5.3	1029.0 ± 11.7
Case II-5	1365.1 ± 9.1	1400.0 ± 7.4	1669.1 ± 16.9
Case II-6	1556.7 ± 12.8	1636.1 ± 9.9	1917.4 ± 21.9

Table 4-11 Measured subcriticality [pcm] deduced by the Noise method

			Subcriticality ρ [pcm] (by Noise method)		
Case	β_{eff} [pcm]	Reference [pcm]	Fiber #1	Fiber #2	Fiber #3
Case II-1	785 ± 4	ρ_{exp} = 1160 ± 5	1491 ± 57	1283 ± 36	2445 ± 105
Case II-2	785 ± 4	ρ_{exp} = 1684 ± 5	2024 ± 28	1814 ± 24	3250 ± 41
Case II-3	783 ± 5	ρ_{exp} = 2483 ± 6	2881 ± 15	2677 ± 11	4203 ± 29
Case II-4	788 ± 5	ρ_{MCNP} = 4812 ± 6	4336 ± 38	4384 ± 35	5740 ± 77
Case II-5	816 ± 5	ρ_{MCNP} = 9895 ± 6	8087 ± 61	8316 ± 50	10110 ± 113
Case II-6	806 ± 5	ρ_{MCNP} = 11556 ± 6	9633 ± 88	10175 ± 68	12096 ± 150

(β_{eff} : MCNP6.1 with JENDL-4.0)

Phase III

Study on Reaction Rates

Appendix-III

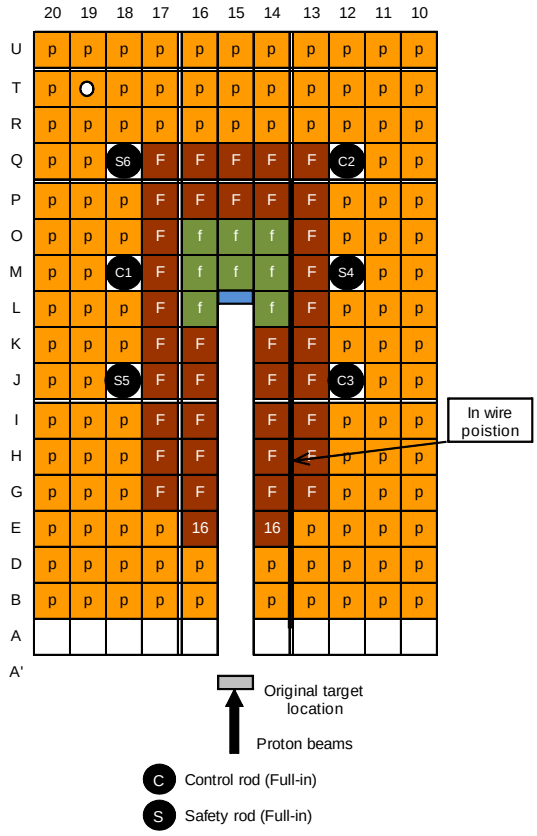

(a) Case II-3 (2483 pcm)

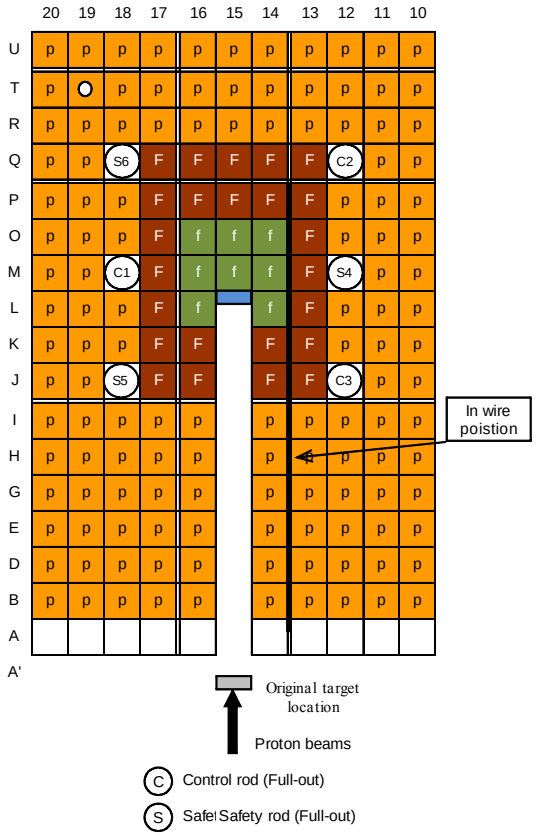

(b) Case II-4 (4812 pcm)

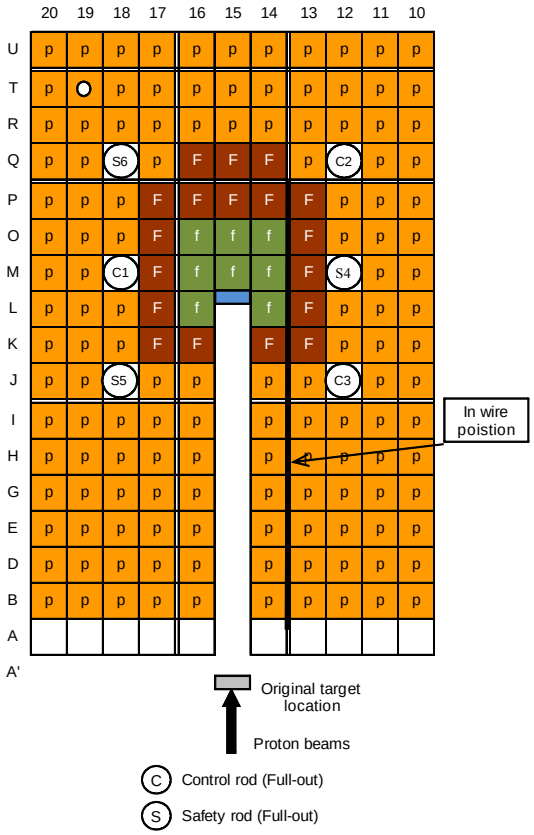

(c) Case II-5 (9895 pcm)

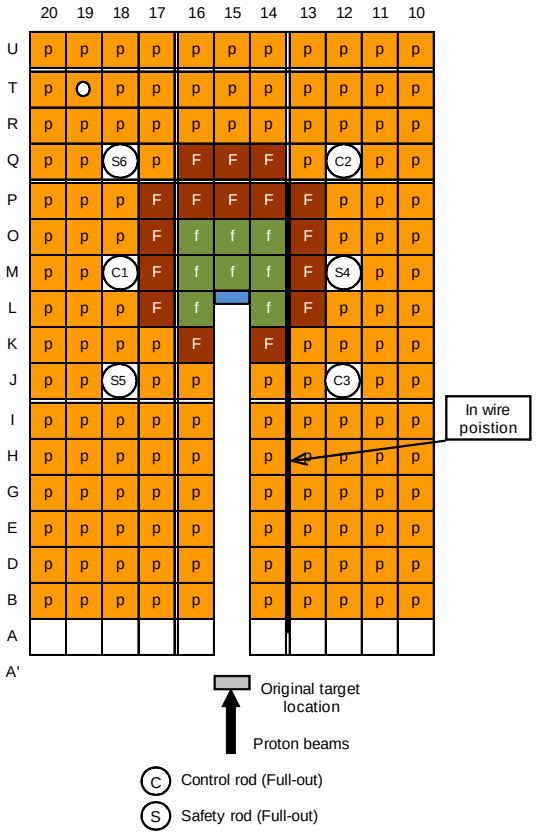

(d) Case II-6 (11556 pcm)

Fig. 5-1 Top view of ^{235}U-fueled and Pb-Bi-zoned ADS core with 100 MeV protons.

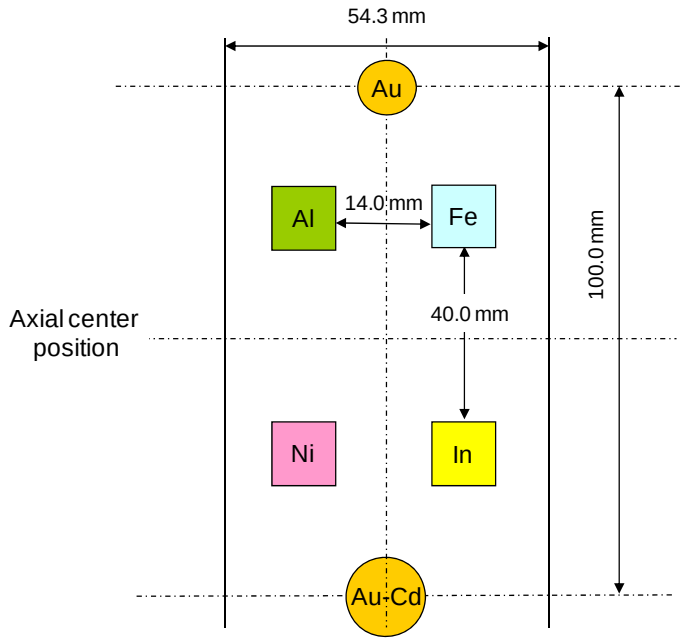

Fig. 5-2 Foil arrangement at a gap between Pb-Bi target and fuel rod in position (15, M) shown in Fig. 4-1

5. Results of Experiments

5-1. Indium Reaction Rate Distribution

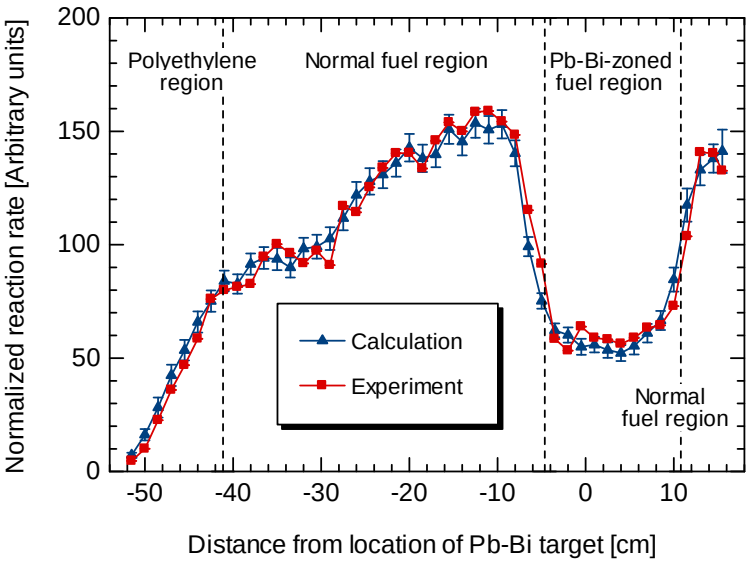

(a) Case II-3

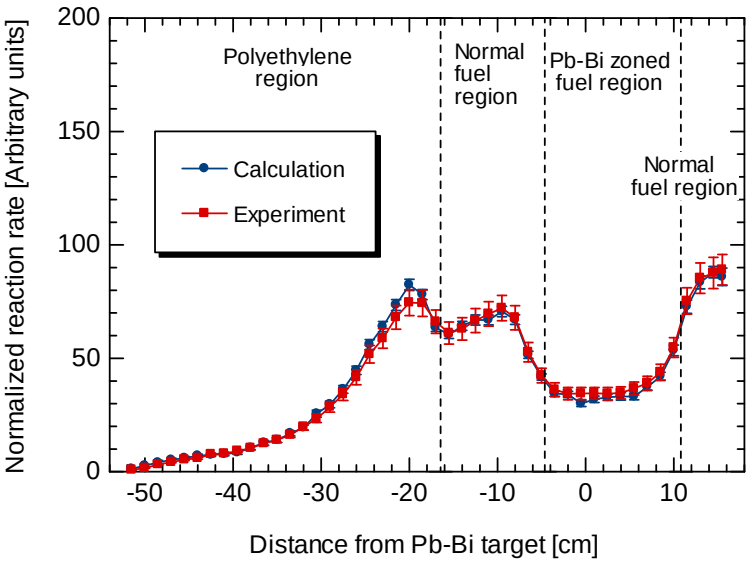

(b) Case II-4

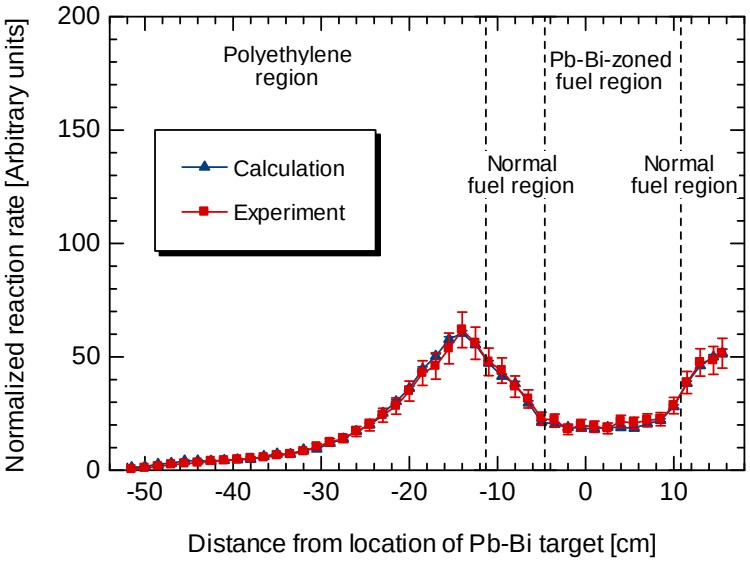

(c) Case II-5

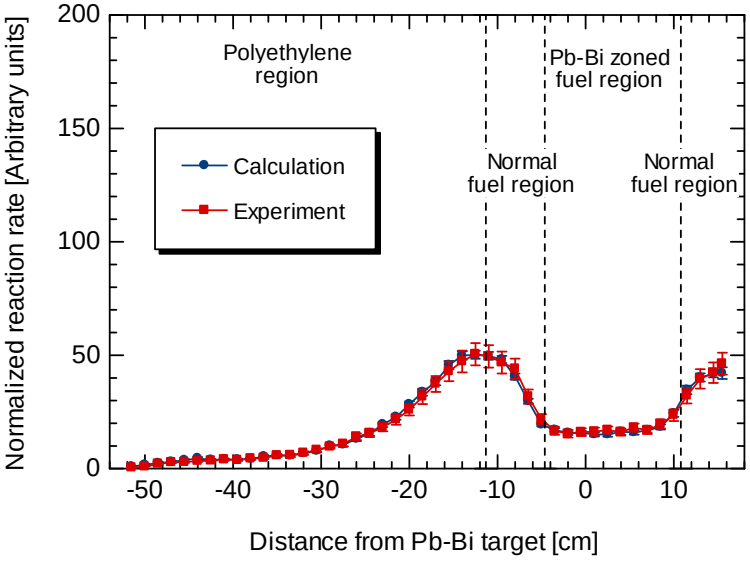

(d) Case II-6

Fig. 5-3 Comparison between measured and calculated $^{115}In(n, \gamma)^{116m}In$ reaction rate distributions along (14-13, P-A) region shown in Figure 1.

5-2. Reaction Rates of Activation Foils

Table 5-1 Main characteristics and description of activation foils.

Reaction	Dimension [mm]	Threshold [MeV]	Half-life	γ-ray energy [keV]	Emission rate [%]
$^{197}Au(n, \gamma)^{198}Au$ (bare and Cd* covered)	8 mm diameter 0.05 mm thick	—	2.697 d	411.9	95.51
Cd plate	10 mm diameter 1 mm thick	—	—	—	—
$^{115}In(n, \gamma)^{116m}In$ (wire)	1 mm diameter 680 mm long	—	54.12 m	1097.3 1293.54	55.7 85
$^{115}In(n, n')^{115m}In$ (foil)	10×10×1	0.4	4.486 h	336.2	45.08
$^{58}Ni(n, p)^{58}Co$	10×10×1	0.9	70.82 d	810.8	99.4
$^{56}Fe(n, p)^{56}Mn$	10×10×1	5.0	2.578 h	846.8 1810.7	98.9 27.2
$^{27}Al(n, \alpha)^{24}Na$	10×10×1	5.6	14.96 h	1368.6	100

Cd*: Au foil (Cd covered) was sandwiched between two Cd plates (10 mm diameter and 1 mm thick).

Table 5-2 Atomic density of activation foils utilized in reaction rates measurement.

Foil	Isotope	Abundance (%)	Purity (%)	Atomic density ($\times 10^{24}$/cm^3)
In	^{113}In	4.3	99.99	1.64406E-03
	^{115}In	95.7	99.99	3.66790E-02
Ni	^{58}Ni	68.27	99.0	6.09388E-02
	^{60}Ni	26.10	99.0	2.41006E-02
	^{61}Ni	1.13	99.0	1.06083E-03
	^{62}Ni	3.59	99.0	3.42546E-03
	^{64}Ni	0.91	99.0	8.96354E-04
Fe	^{54}Fe	5.82	99.99	4.83829E-03
	^{56}Fe	91.18	99.99	7.79975E-02
	^{57}Fe	2.1	99.99	1.81771E-03
	^{58}Fe	0.28	99.99	2.46635E-04
^{27}Al	^{27}Al	100	99.0	5.99156E-02
^{197}Au	^{197}Au	100	99.95	5.90193E-02

Table 5-3 Measured reaction rates of activation foils in Cases II-3 through II-6.

	Measured reaction rate [1/s/cm^3]			
Reaction	Case II-3	Case II-4	Case II-5	Case II-6
^{197}Au(n, γ)^{198}Au (bare)	(8.88 ± 0.02)E+06	(4.88 ± 0.04)E+06	(3.51 ± 0.08)E+06	(2.53 ± 0.04)E+06
^{197}Au(n, γ)^{198}Au (Cd)	(7.84 ± 0.09)E+06	(4.46 ± 0.04)E+6	(3.11 ± 0.04)E+6	(2.30 ± 0.03)E+06
^{115}In(n, n')^{115m}In	(8.60 ± 0.13)E+04	(4.27 ± 0.22)E+04	(4.27 ± 0.03)E+04	(2.86 ± 0.06)E+04
^{58}Ni(n, p)^{58}Co	(4.90 ± 0.08)E+04	(3.18 ± 0.03)E+04	(3.23 ± 0.16)E+04	(2.00 ± 0.10)E+04
^{56}Fe(n, p)^{56}Mn	(1.82 ± 0.07)E+03	(1.26 ± 0.02)E+03	(1.55 ± 0.03)E+03	(1.39 ± 0.02)E+03
^{27}Al(n, α)^{24}Na	(1.54 ± 0.05)E+03	(1.11 ± 0.02)E+03	(1.62 ± 0.03)E+03	(1.10 ± 0.01)E+03